UCID-20512

A Model of Hydrocarbon Maturation in the Uinta Basin, Northeastern Utah

J. J. Sweeney
A. K. Burnham
R. L. Braun

AUGUST 1985

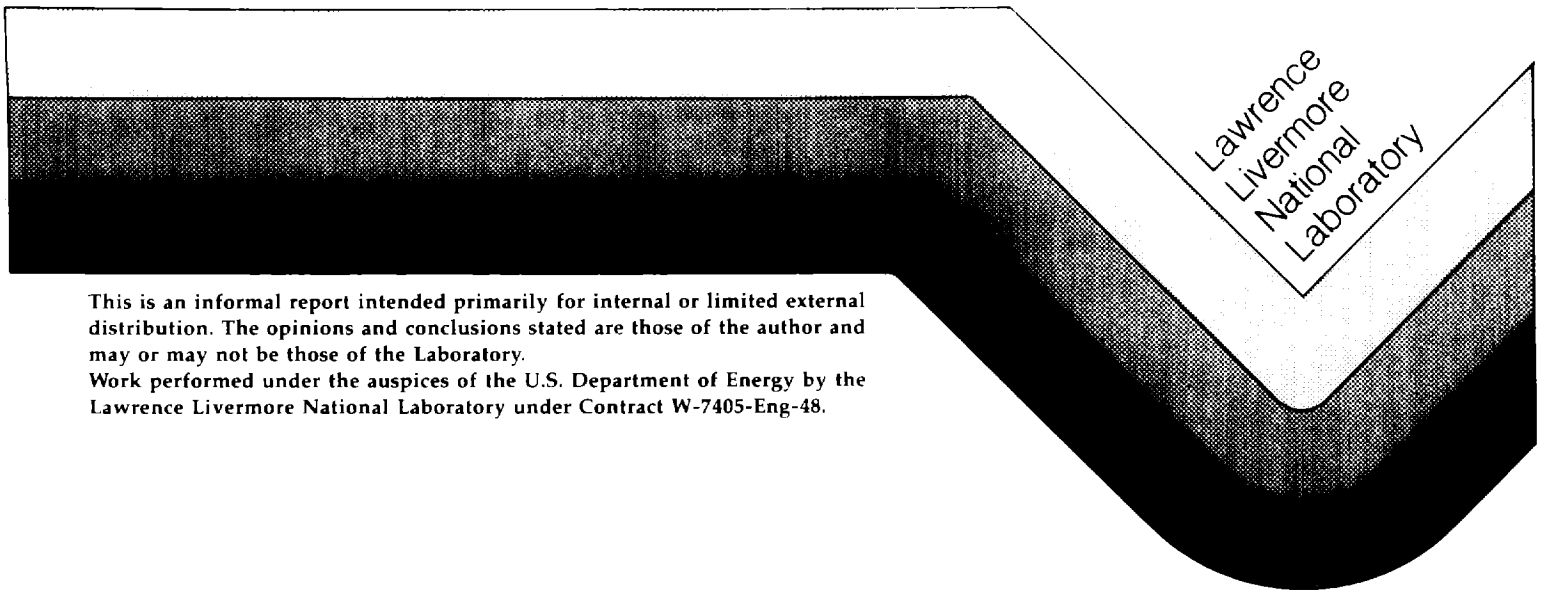

DISCLAIMER

Printed in the United States of America
Available from
National Technical Information Service
U.S. Department of Commerce
5285 Port Royal Road
Springfield, VA 22161
Price: Printed Copy $ Microfiche $4.00

Page Range	Domestic Price	Page Range	Domestic Price
001-025	$ 7.00	326-350	$ 26.50
026-050	8.50	351-375	28.00
051-075	10.00	376-400	29.50
076-100	11.50	401-426	31.00
101-125	13.00	427-450	32.50
126-150	14.50	451-475	34.00
151-175	16.00	476-500	35.50
176-200	17.50	501-525	37.00
201-225	19.00	526-550	38.50
226-250	20.50	551-575	40.00
251-275	22.00	576-600	41.50
276-300	23.50	601-up[1]	
301-325	25.00		

[1]Add 1.50 for each additional 25 page increment, or portion thereof from 601 pages up.

Table of Contents

ABSTRACT

Lawrence Livermore National Laboratory has been carrying out pyrolysis experiments on Green River oil shale (Type I kerogen) for many years. A computer model has been developed to determine the fractions and relative compositions of solid and liquid hydrocarbons and volatiles developed at heating rates and temperatures present in an oil shale retort. A thermal model of the development of the Uinta Basin in Utah has also been developed to see if the kerogen pyrolysis model is valid when extrapolated to temperatures and heating rates on a geologic scale. Geophysical log data from the Altamont-Bluebell and Redwash oil fields in the Uinta Basin have been used to develop a model of the thermal history of Green River Formation stratigraphic intervals which contain Type I kerogen. The basin thermal history data, in the form of heating rates and maximum temperatures attained as a function of time, were put into the kerogen pyrolysis model to compute compositional changes in the oil and gas fraction with time. Initial results show good qualitative agreement between calculated values and actual oil compositions from published data. Uncertainties in the geologic model result from incomplete information concerning lithologic ages, timing of events, and geophysical data such as density, porosity, and thermal and pressure gradients. The inherent uncertainty in the pyrolysis model arises from simplifying assumptions made and the fact that the heating rates modeled are about nine orders of magnitude slower than rates in laboratory experiments. We feel, however, that the general agreement of these two approaches in this analysis of hydrocarbon evolution lends credence to both models. The successful application of the kerogen pyrolysis model demonstrates the utility of the approach used here as a tool in the analysis of the thermal history of geologic basins, although further experiments and model development would be required to extend the application to Type II and III kerogens.

I. Introduction

The Uinta Basin in northeastern Utah provides an ideal setting to study the evolution of kerogen to petroleum. Oil shale rocks of the Eocene-age Green River Formation outcrop extensively at the southern edge of the synclinal basin. The same rocks are also found at depths of 3650 m in the deepest part of the syncline. Mature petroleum is presently being recovered from these deeply buried rocks, so we know that kerogen has been converted to petroleum within the basin.

The term "oil shale," as generally used here, refers to fine-grained rock which contains a large amount of organic material. From geological studies (Bradley, 1925, 1931, 1970; Andersen and Picard, 1974; Fouch, 1975; and Ryder, et al., 1976) it is generally accepted that the Green River Formation rocks were formed in a lacustrine environment which commenced in the mid to late Paleocene and reached its maximum extent in mid Eocene time. Organic and inorganic matter was deposited in varying proportions in yearly cycles, creating varves that can be traced over miles (Bradley, 1929; Smith, 1974). The organic material is diagenetically changed from its original form and is mostly in an insoluble form called kerogen. Petrographic studies indicate that most of the kerogen is amorphous (Bradley, 1925; Robinson, 1969). The kerogen is most likely derived from the lipid fraction of lake algae and from terrestrial spores and pollen (Yen, 1976). It is a classic example of a Type I kerogen in the classification scheme of Tissot and Welte (1978).

Oil shale from the Green River Formation have been studied in pyrolysis experiments for many years at Lawrence Livermore National Laboratory (LLNL). The purpose of these experiments has been to better understand the process of extraction and to calculate rates and amounts of oil formation for a variety of pyrolysis conditions. Most recently we have developed a detailed computer model that can accurately predict the rates and amounts of chemical products (or species) developed at heating rates, temperatures, and pressures prevalent in different kinds of oil shale retort processes (Burnham and Braun, 1985). Data used in the development of this model are from laboratory measurements of Burnham and Singleton (1983), which incorporated heating rates ranging from 1°C to 100°C per hour, and pressures of 0.1 to 2.7 MPa. The model works well

within this range. A test of the fundamental accuracy of this model is provided by extending the range of application to lower heating rates and temperatures. We have done this by applying a specific temperature history of a geological basin, which is producer of mature petroleum and natural gas, to the kerogen pyrolysis model.

In this paper geophysical and geological data from the Uinta Basin are used to develop a time-temperature history of the kerogen-rich rocks of the Uinta Basin in Utah. This time-temperature model is then used to characterize, via pyrolysis model calculations, conversion of kerogen to various hydrocarbon products through time. The end result is a prediction of the present-day kerogen maturity level for various depths and locations within the Altamont-Bluebell and Redwash oil fields of the Uinta Basin. We then compare these results with maturity data based on material extracted from the same oil fields.

II. Geologic Setting and History

A. Geology of the Uinta Basin

The Uinta Basin is a structural and topographic depression in the northeastern corner of Utah (Fig. 1). The topographic low is surrounded by the Uinta Mountains to the north, Wasatch Mountains to the west, San Rafael Swell and Uncompahgre Uplift to the south, and the Douglas Creek Arch to the east. Relief between the lowest part of the surface of the basin and the surrounding highlands ranges from 900 to 1800 m.

Hydrocarbon production occurs in Paleozoic, Mesozoic, and Cenozoic formations in the Uinta Basin. Only the Cenozoic part of the basin, in which an extensive lacustrine environment was in evidence by the beginning of the Paleocene Epoch, is of concern in this study. During the early Tertiary as much as 6000 m of lacustrine and alluvial sediments were deposited. The sediments represent a central core of open lacustrine claystone and carbonate mudstones; a marginal lacustrine facies with sandstone, claystone, and

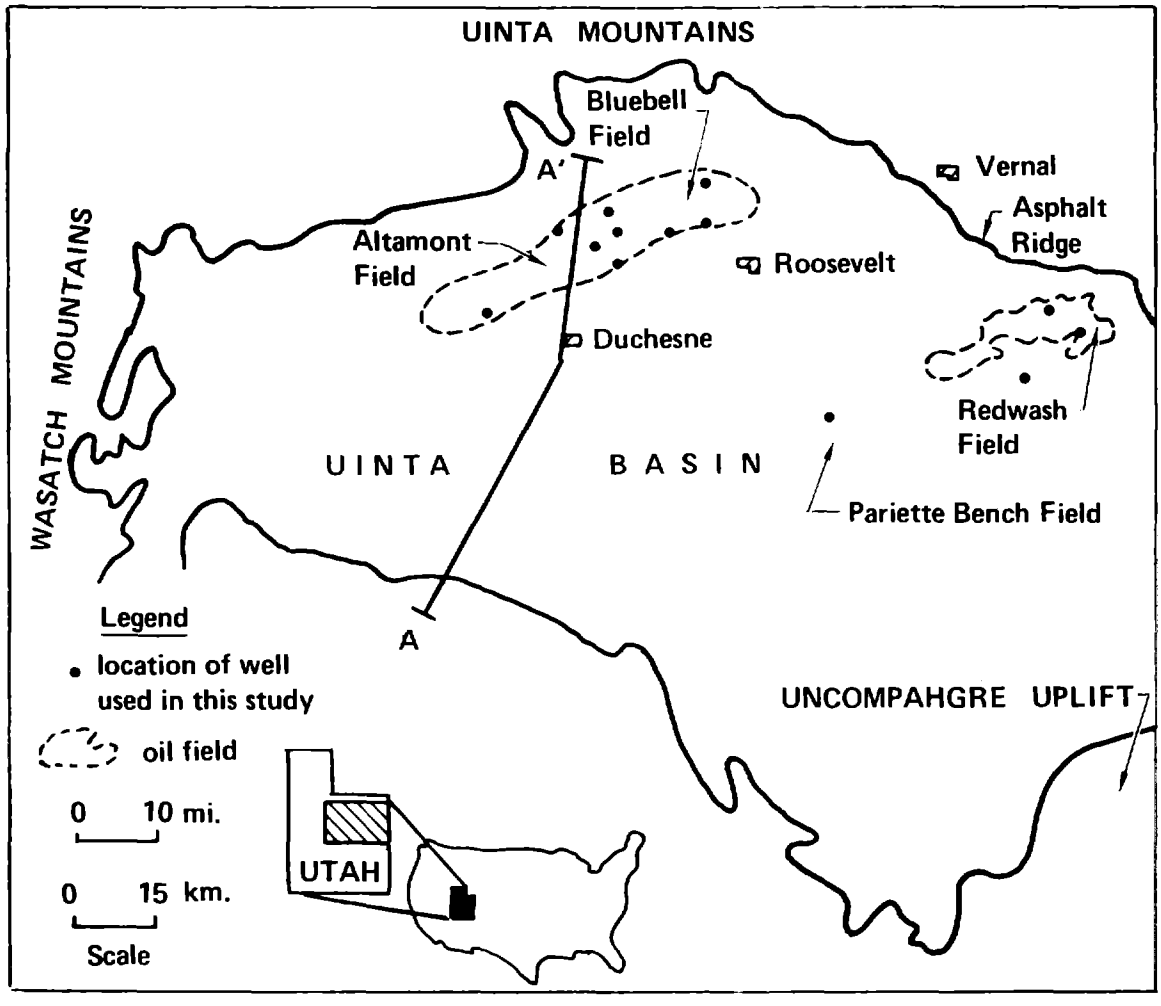

Figure 1: Map of the Uinta Basin showing locations of the Altamont-Bluebell and Redwash oil fields. Line A-A'shows the location of the cross-section of Figure 2.

carbonate; and peripheral alluvial facies of conglomerate, claystone, and carbonaceous shale (Fouch, 1975). The lacustrine period of deposition waned in the late Eocene and later deposition was primarily alluvial in character.

Structurally the basin is a simple asymmetric syncline with an east-west trending axis near the northern side. Dips on the north limb are 10 to 35 degrees, while they are only 2 to 4 degrees on the south limb (Fig. 2). In contrast to the structural simplicity, stratigraphic relations are complex, but marker units can be traced throughout the basin.

Two specific oil fields in the basin were selected for analysis in this study because of their differing characteristics and because of the availability of a large amount of data from drilling. The Altamont-Bluebell field (Fig. 1), described by Lucas and Drexler (1975), has production of oil and gas from multiple thin reservoirs in the lower Tertiary section at depths of 2400 to 3600 m. Traps are in fractured sandstone with stratigraphic pinchouts which are overpressured in the main producing area. The Redwash field is located about 40 miles (64 km) to the east of the Altamont-Bluebell field. Production at Redwash is from fractured sandstone lenses located in the lower part of the Eocene Green River Formation at depths of 1500 to 1800 m (Chatfield, 1972). Both of these fields produce oil and gas derived from lacustrine rocks at similar stratigraphic levels, but the present depth of burial of these producing zones varies considerably.

B. Stratigraphy and Ages of Units

In order to develop a model of the thermal history of lithologic units in a basin, the burial history must be known. The key factor in developing a burial history is establishment of basin-wide stratigraphic markers for which good age control is available. The complex interfingering stratigraphy of the Green River Formation of the Uinta Basin makes this difficult. Fortunately, a series of correlation markers has been established by Fouch (1975).

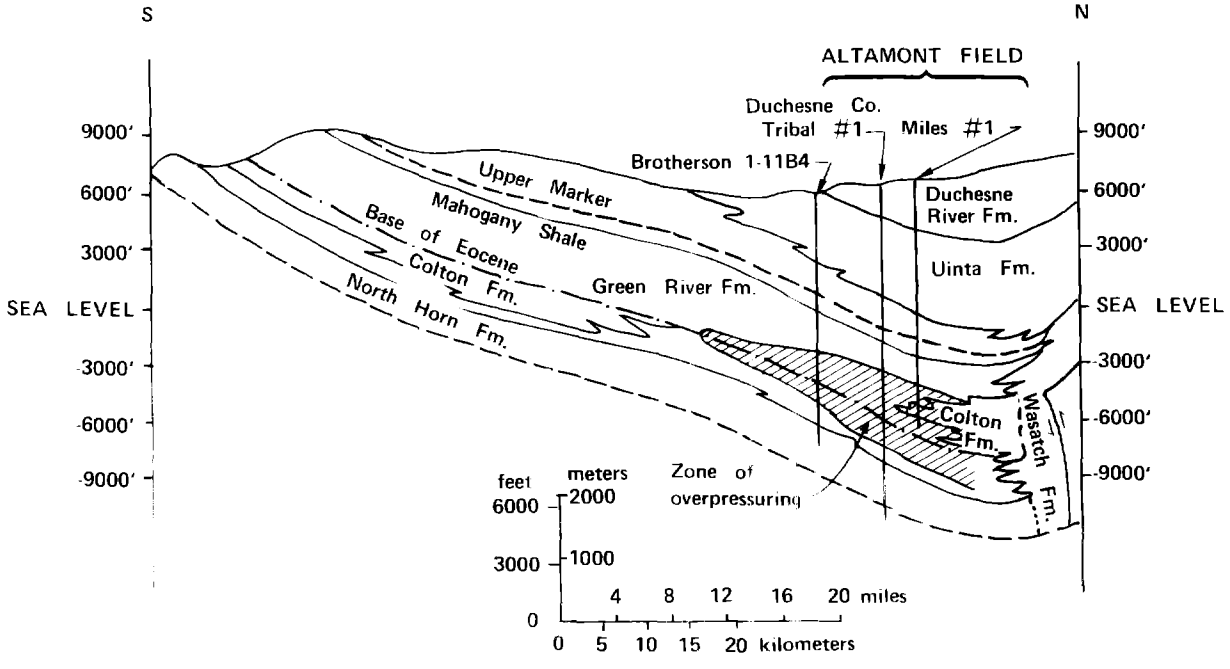

Figure 2: Cross section from south to north across the central part of the Uinta Basin (after Fouch, 1975).

The base of the Tertiary sequence of the Uinta Basin begins with the Upper Cretaceous to Paleocene North Horn Formation (see Fig. 2). The overlying Paleocene to Eocene Green River Formation consists of the central lacustrine facies which interfingers with the marginal and peripheral facies of the Colton and Wasatch Formations. Markers identified by Fouch (1975) are 1) the lower marker, 2) the Paleocene-Eocene boundary, 3) the top of the carbonate marker unit, 4) the middle marker, 5) the Mahogany oil-shale bed, and 6) the upper marker.

Green River Formation is overlain by the Uinta and Duchesne River Formations. These formations are fluvial deposits which mark the demise of lacustrine conditions and an inception of Laramide tectonic activity (Andersen and Picard, 1974). The Duchesne River and upper parts of the Uinta Formation have been eroded away from some parts of the basin and are exposed in places near the Altamont-Bluebell and Redwash oil fields. The Oligocene Bishop Conglomerate and Oligocene to Miocene Browns Park Formation, which overlie the Duchesne River Formation, occur in the area surrounding the Uinta Mountains, but are largely eroded from the Uinta Basin. The Bishop Conglomerate is considered by Hansen (1984) to be correlative in age to the upper part of the Duchesne River Formation. The Bishop probably formed a wide continuous bajada around the Uinta range, reaching the centers of the surrounding basins during a long period of crustal and climatic stability beginning in the Oligocene (Hansen, 1984).

The beginning of Tertiary time has been placed at 66.4 million years ago (My), with the Paleocene-Eocene boundary at 57.8 My (Decade of North American Geology Time Scale, Palmer, 1983). Dating using K-Ar ages of biotite in tuff (Mauger, 1977) suggests an age of about 45.0 My for the Mahogany oil-shale unit, with the base of the Uinta Formation at about 44.0 My. The uppermost part of the Uinta Formation is estimated by Mauger (1977) to be about 41.0 My. Andersen and Picard (1974) estimate that the uppermost part of the Duchesne River Formation, the Starr Flat Member, may be as young as Oligocene. Hansen (1984) considers part of the Bishop Conglomerate as equivalent to the Starr Flat Member. Tuff in the Bishop Conglomerate has been dated at 29.0 My (Hansen, 1984). The period of stability which began about

29 My extended up into the Miocene, when renewed uplift resulted in downcutting and deposition of the Browns Park Formation. Tuffs in the upper part of the Browns Park are 8-12 My in age (Hansen, 1984). Uplift and erosion have continued into the Quaternary.

C. The Geologic Model

From the stratigraphic and age data given above a simple geologic model of the basin history has been developed. The time events chosen for the model, in million years before present (My), are as follows:

Event	Time Period
Renewed Uplift	10 My - present
Period of stability and peneplanation	30 My - 10 My
Deposition of Duchesne River Formation and Bishop Conglomerate	41 My - 30 My
Deposition of Uinta Formation	44 My - 41 My
Deposition of Mahogany Oil-Shale	45 My
Paleocene-Eocene boundary	57.8 My

We decided that this simple model was an appropriate "first cut" to use in comparing the geological and geochemical models. We assumed that deposition rates were uniform throughout. The model thus represents a time averaging of the actual, more complicated, depositional history. Ages used in the model are not solidly constrained by geologic data, so the numbers used are what we consider a best estimate. We consider this model to be a working model which can be adjusted and modified as further study warrants.

The next step in determining the burial history of the basin is to establish the history of the thickness and burial depth of the stratigraphic units of the model. Present burial depths can be determined from borehole lithologic correlations, but present burial depths do not represent the

maximum depth of burial because a considerable amount of uplift and erosion of the basin has occurred. Determination of the amount of overburden removed in the basin is a crucial part of the analysis.

III. Basin Analysis and Development of the Burial History

A. Previous Work

Previous studies most pertinent to this work are those of Reed and Henderson (1971), Tissot et al. (1978), and Anders and Gerrild (1984). Reed and Henderson analyzed crude oil from nine fields in the Uinta Basin, including Redwash and Pariette Bench, for alkane and elemental compositions. In their work they found strong evidence for stratigraphic control of crude oil composition and concluded that the oil shales have not been the dominant source-rocks of the reservoired petroleum. The study by Tissot et al. (1978), showed that the lower part of the Green River Formation is in the principal stage of oil generation and responsible for most of the crude oils produced. Anders and Gerrild (1984) compared variations in the compositions of organic material from the Altamont-Bluebell area with location, depositional environment, and thermal maturation.

An analysis of the historical stress regime for the Altamont Field was computed by Narr and Currie (1982). They found evidence that fractures developed in the basin only after burial to the maximum depth and that fracturing continued throughout the subsequent period of uplift and erosion. Pitman et al. (1982) found the Green River Formation at the Pariette Bench Field to be thermochemically immature and not the source of production. They suggest that the oil found at Pariette Bench migrated through a network of fractures from the Bluebell-Altamont area. Anders and Gerrild (1984) also conclude that migrated oil is present in the Pariette Bench area as well as in other parts of the basin.

The findings cited above show apparent contradictions which are related to the fact that oil in various fields may have different sources. The Altamont-Bluebell, Redwash, and Pariette fields contain Green River Formation rocks at different present-day burial depths and have different burial

histories. The intent of this study is to integrate information about geological and geochemical evolution of the rocks in each field to evaluate the oil generation potential. Knowledge of the oil generation potential at each field will then allow assessment of the possible contribution of migrated oil to the field production.

B. Procedure for Calculating Burial History

The complete burial history of a basin is determined from the maximum depth of burial and the thickness of each stratigraphic unit through time. The time-thickness relation can be determined from the density or porosity of the unit as a function of burial depth and from the burial history using a method known as backstripping (Sclater and Christie, 1980; Steckler and Watts, 1978). In the process of backstripping, units above the stratigraphic level of interest are mathematically removed from top to bottom and the uncompacted thickness is calculated as a function of burial depth (and time). The end result is an estimate of the burial depth of a particular stratigraphic level throughout its history. With knowledge or estimates of past geothermal gradients we can then calculate the time-temperature relation.

Geologic evidence indicates that a considerable part of the stratigraphic section has been eroded from the Uinta Basin. The Duchesne River Formation and the upper part of the Uinta Formation are exposed at the surface in some parts of the basin (Stokes, 1963). Outcrops of the Browns Park Formation occur as much as 1825 m above the basin floor. Narr and Currie (1982) take this difference to be representative of the amount of sediment removed from the basin. Analysis of fluid inclusion data from core from the Altamont field by Narr and Currie (1982) led to estimates of 510 to 2890 m of overburden removed. Tissot et al. (1978) use 1780 m for the amount of erosion at the Shell Brotherson 1-23-B4 well, Altamont field, but they do not say how the value was determined. Pitman et al. (1982), from reconstructed thicknesses of the Uinta and Duchesne River Formations, estimate a maximum of 1000 m of overburden removal in the Pariette Bench Field, to the southeast of the Altamont Field.

Differences of 2380 m in estimates of the amount of removed overburden can have a major influence on estimates of the maximum depth of burial and hence the maximum temperatures attained by kerogen-bearing rocks in the basin. Because of the alluvial nature of the Uinta and overlying formations, reconstruction of overburden thickness for various parts of the basin is extremely difficult. One way to attempt to solve this problem is to incorporate a method which uses borehole interval velocity data, as demonstrated by Magara (1978). This method is explained below.

C. Estimation of Amount of Removed Overburden

The relationship between porosity and depth of burial for shales and argillaceous rocks is illustrated by Magara (1978). Because interval velocity is related to density, there is a corresponding velocity-depth relation. In study of the Cretaceous shales of western Canada, Magara found what he termed a "normal compaction trend" relating depth and interval travel time. The normal compaction trend occurs as a linear curve on a logarithmic-scale plot of interval transit time versus linear depth. A representative curve is shown in Fig. 3a. The normal compaction curve thus gives a representative value of interval velocity corresponding to a given depth of burial, assuming no post-depositional erosion. The zero-depth intercept, Δt_0, is the transit time of mud-saturated water, usually taken to be 200 μs/ft.

Magara (1978) demonstrates how to use the normal compaction curve to determine the amount of overburden removed (see Fig. 3b). When overburden has been removed from the area of the borehole, the zero-depth intercept will no longer be at Δt_0, but at some lesser value, $\Delta t'_0$, depending on the amount of removed overburden. The procedure involves determining the normal compaction trend from an area with little or no erosion and then fitting that curve to data from a nearby area where erosion has taken place. From $\Delta t'_0$ at the well in question the thickness of the removed overburden can be calculated. The problem with applying this method to the Uinta Basin is that erosion has taken place everywhere. Thus a normal compaction curve can only be determined by averaging the slopes of a number of interval velocity-depth logs.

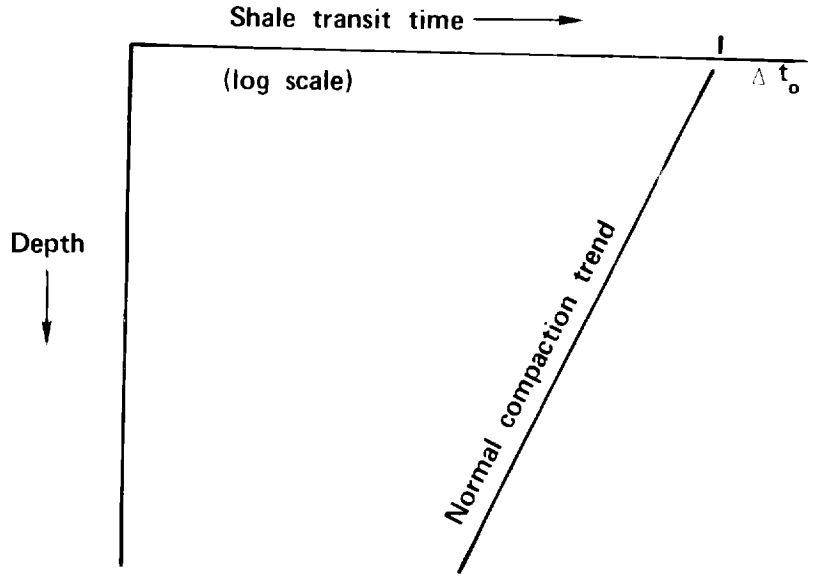

Figure 3a: A generalized transit time-depth plot for the case where no erosion has occurred.

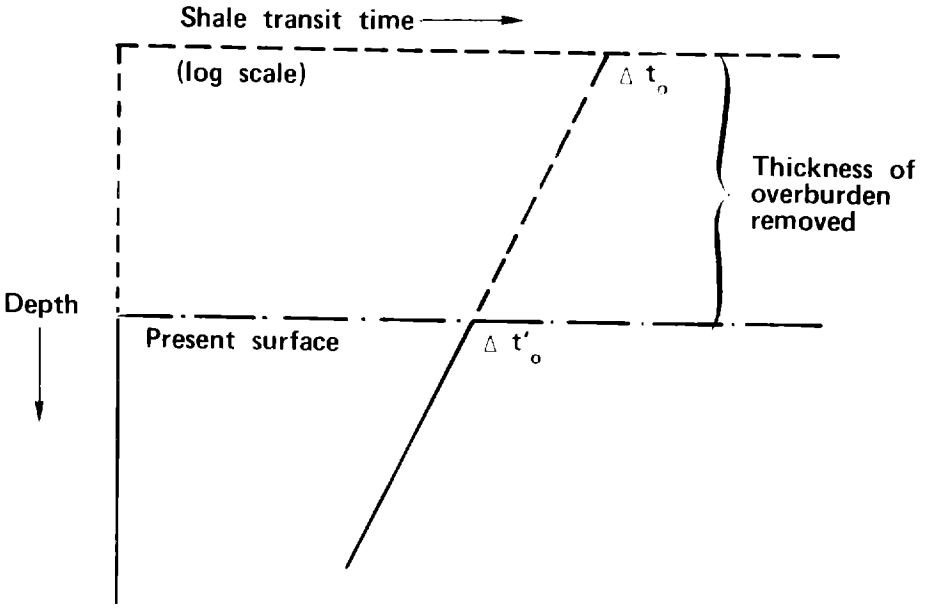

Figure 3b: Transit time-depth plot for the case where erosion has occurred. The transit time extrapolated to zero depth in this case is $\Delta t'_0$.

Down-hole acoustic logs (DHAL), which give a measure of interval velocity versus depth, are commonly run in petroleum exploration. Electric logs, also commonly run, can be used to estimate the shale content as signified by zones of low resistivity. For this study, we obtained DHAL and E-logs for a representative number of wells in or near the Altamont-Bluebell, Pariette Bench, and Redwash Fields. In each case we used the E-log to identify shale-rich zones which were then matched with depths on the DHAL to obtain interval velocities.

We picked well locations where detailed lithologic data were available from previously published work (Narr and Currie, 1982; Pitman et al., 1982; Tissot et al., 1978; Reed and Henderson, 1971; Fouch, 1981; and Fouch and Cashion, 1979) and obtained a suite of logs which provided data over a depth interval of at least 1525-2440 m. Locations of these wells are shown in Fig. 1.

A linear fit to a semi-log plot of Δt versus depth (z) data has the form

$$\log \Delta t = a - bz. \tag{1}$$

Magara (1978) also uses the equation

$$\Delta t = \Delta t_o e^{-cz} \tag{2}$$

for the expression relating the transit time to burial depth. The relationship of the parameters in (1) and (2) is

$$\Delta t_o = 10^a \tag{3}$$

$$c = b \ln 10 = 2.303b. \tag{4}$$

Once the normal compaction trend (values of c or b deemed typical of the basin) is determined, individual Δt-z plots are used to determine $\Delta t'_o$, and hence the amount of overburden removed by erosion.

When b is given, the intercept a is determined by least squares fit for a given set of log data from

$$a = \frac{1}{n}\left[\sum_{n} \log \Delta t_i + b\sum_{n} z_i\right] . \qquad (5)$$

where n is the number of data points. Using (3), $\Delta t'_o$ is found, and the amount of overburden removed, Z_{OB}, is determined from

$$Z_{OB} = \frac{1}{b} \log \frac{200}{\Delta t'_o} . \qquad (6)$$

In this case 200 μs/ft is assumed to be the interval transit time for mud saturated water at zero depth.

Caution must be used when using the Δt - z plots because of the possibility of present day or past overpressures at depth which lead to undercompaction of shale and a corresponding roll-off of interval transit time (Magara, 1978). This is seen in most logs from the Uinta Basin. Figures 4 and 5 are Δt - z plots from typical borehole data. The Gulf Duchesne County and Shell-Tenneco-Brotherson wells are from the Altamont-Bluebell field. The Chorney Oil South Redwash well is in the Redwash field. Note that below depths of 5000 to 6000 ft (1500 to 1800 m), interval transit time begins to increase with depth and then varies up and down in a cyclic fashion. Thus only the portion of the curve above 6000 ft (1800 m) depth has been used to determine a and b.

As mentioned above, erosion has occurred over all portions of the Uinta Basin. Thus there is no area where a true normal compaction trend extends to 200 μs/ft at z = 0. For this study we estimated a normal compaction trend by averaging the slopes from a number of curves. We determined normal compaction curve slopes for seven wells from the Altamont-Bluebell field, one well from the Redwash field, and one well at Pariette Bench. Well names, number of data points used, and the value of b and c calculated for the curves (determined by a least-squares linear curve fit) are given in Table 1.

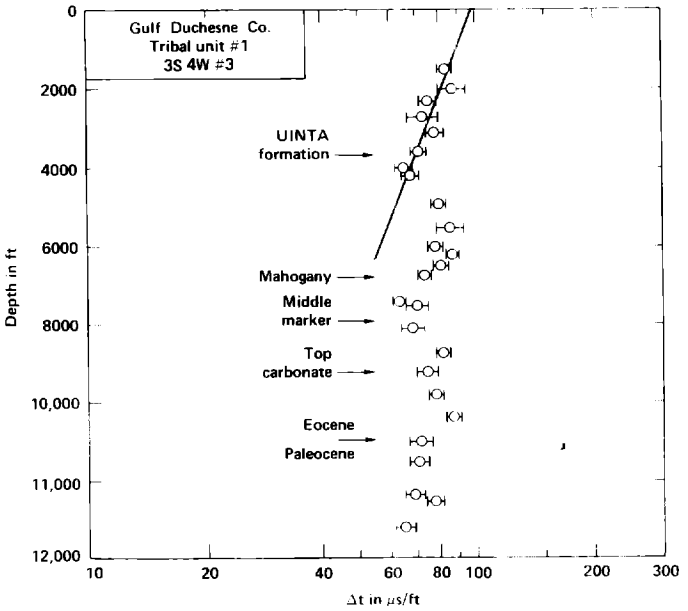

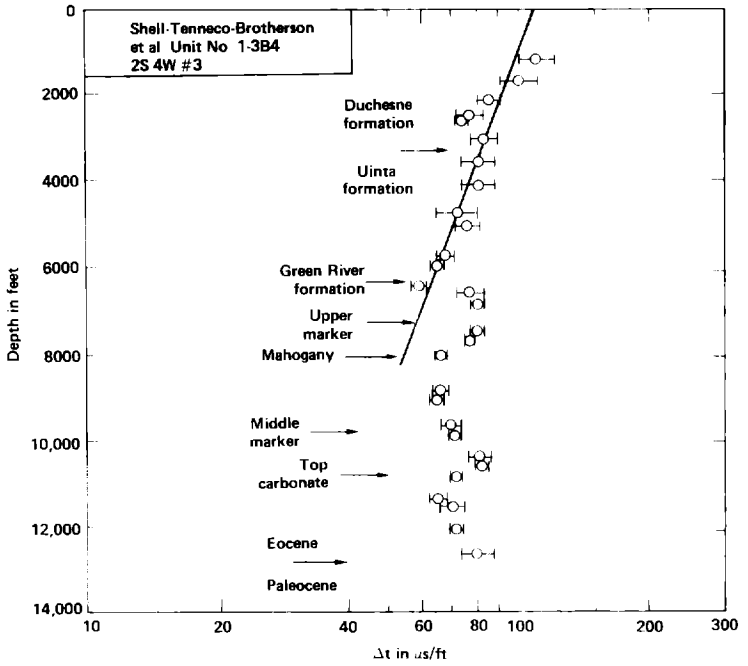

Figure 4: Interval transit time-depth plot for wells in the Altamont-Bluebell field. Stratigraphic location markers are for present-day locations in the wells.

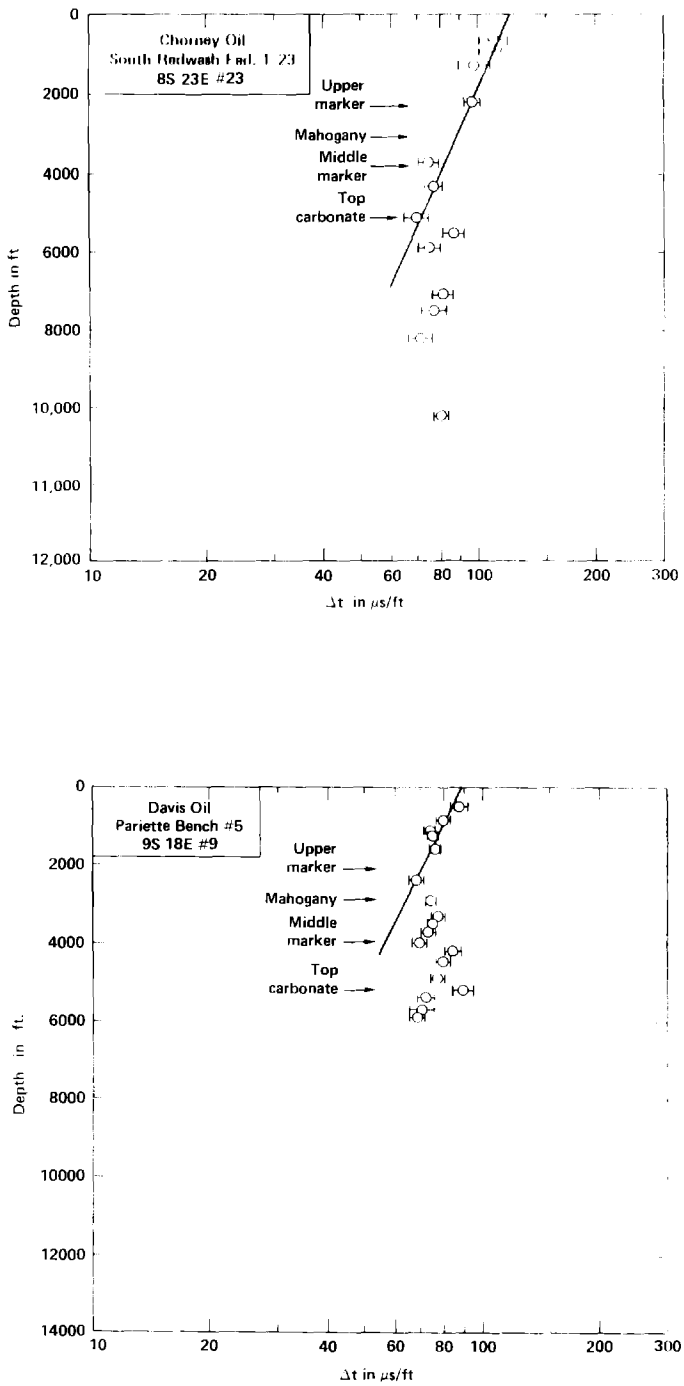

Figure 5: Interval transit time-depth plot for wells in the Redwash field and Pariette Bench field. Stratigraphic location markers are for present-day locations in the well.

TABLE 1: Data used to estimate a normal compaction curve for the Uinta Basin.

Well	No. of pts.	b (ft^{-1})	c (ft^{-1})
Shell Christensen	13	3.203×10^{-5}	0.000074
Shell-Tenneco-Brotherson	13	3.761×10^{-5}	0.000087
Pariette Bench	6	4.982×10^{-5}	0.000115
Chorney S. Redwash	7	4.904×10^{-5}	0.000113
Chevron Ute Tribal	8	4.904×10^{-5}	0.000113
Shell Brotherson 1-11B4	10	3.997×10^{-5}	0.000092
Broadhurst	14	4.484×10^{-5}	0.000103
Gulf Verl Johnson	6	3.441×10^{-5}	0.000079
Duchesne Trial	8	3.822×10^{-5}	0.000088
Average	9.44	4.166×10^{-5}	0.000096

$\sigma_b = 0.673 \times 10^{-5}$ ft^{-1} (standard deviation of b)

The average value for c of .000096 ft^{-1} is within the range of .000085 to .000147 ft^{-1} which Magara (1978) obtained for Cretaceous shales in western Canada. The lower values of c obtained by Magara were for the youngest rocks.

We used the average value for b obtained above to determine $\Delta t'_0$ and Z_{OB} using equations (3), (5), and (6) and borehole log data from the basin (plots similar to Fig. 4). Results for 13 wells in the Uinta Basin are given in Table 2. Values of Z_{OB} corresponding to a plus or minus one standard deviation change in b are also given. These numbers show that the uncertainty in the estimate of Z_{OB} due to uncertainty in b is about $\pm$ 300 m. Note from the table that lower values of Z_{OB} are obtained from wells in Redwash field (Chevron Redwash, Chorney South Redwash, and #13 Broadhurst). The highest value of Z_{OB} is from the Pariette Bench #5 well. Figure 6 shows the variation in Z_{OB} throughout the Altamont-Bluebell area. Values of Z_{OB} range from 1800-2000 m except for Gulf Verl Johnson (1598 m) and Duchesne Tribal (2252 m).

TABLE 2: Calculated values of Z_{OB}, in meters, for well locations in the Uinta Basin. A range of values is calculated for a range of one standard deviation of the slope parameter, b.

Well & Location	$\Delta t'_o$ (μs/ft)	Using b	Range	Values Determined by Narr & Currie (1982)
Energy Res. Gp. Broadhurst #13, 7S22E#9	113.41	1802	1552-2150	---
Shell Christensen 1-33A5, 1S5W#33	107.01	1987	1711-2370	1733
Shell Tenneco-Brotherson 1-3B4, 2S4W#3	110.86	1875	1614-2336	510
Gulf Duchesne Co Unit 1, 3S4W#3	98.44	2252	1939-2687	---
Davis Oil Pariette Bench #5, 9S18E#9	86.22	2673	2302-3189	---
Gulf Verl Johnson #1, 1S2W#27	120.96	1598	1376-1906	2850 1338 756
Shell Brotherson 1-11B4, 2S4W#11	113.63	1796	1547-2142	1968
Chevron Ute Tribal 6-7, 2S3W#7	111.09	1868	1608-2228	---
Chorney Oil S. Redwash Fed. 1-23, 8S23E#23	116.18	1726	1486-2058	---
Shell Miles #1, 1S4W#35	112.28	1834	1579-2188	339 583
Gulf Ute Tribal 1-21, 1N2W#21	107.44	1974	1700-2355	---
Texaco Ute Tribal E-1, 3S6W#12	110.73	1878	1617-2241	---
Chevron Redwash 250, 7S24E#29	128.34	1410	1519-1681	---

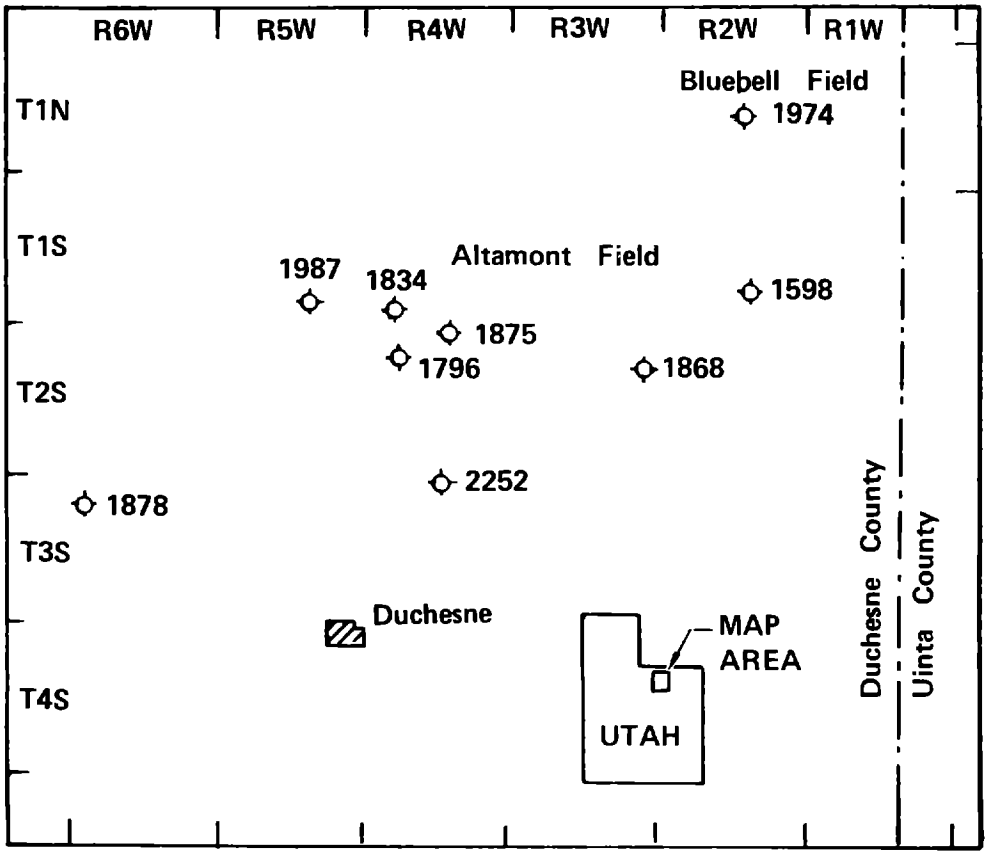

Figure 6: Locations of wells in the Altamont-Bluebell field area used in this study (see also Fig. 1). The calculated amount of removed overburden, in meters from Table 2, is listed next to each well.

Estimates of Z_{OB} from fluid inclusion data by Narr and Currie (1978) are also listed in Table 2 for comparison with this study. The values of Z_{OB} for the Shell Christensen and Shell Brotherson wells determined by Narr and Currie roughly agree with values determined here. Other values of Narr and Currie are either very low or very high compared to our estimates. Tissot et al. (1978) give a value of 1780 m of overburden removed at the Shell Brotherson 1-23B4 well in Sect. 23, 2S, 4W. They do not explain how the value was determined, but it agrees well with values of 1875 m (Sect. 3, 2S, 4W) and 1796 m (Sect. 11, 2S, 4W) given in Table 2.

The assumption is made in equation (6) that the zero-depth interval transit time for water saturated mud is 200 μs/ft (corresponding to a velocity of 1.52 km/s - 5000 ft/s). Magara (1978) found this value to work well for data from Cretaceous shales in Canada. It also corresponds to typical velocities of water-saturated fine to medium silt (Carmichael, 1982). Carmichael also lists velocities of 1.47 to 1.54 km/s (4823 to 5052 ft/s) for compacted terrigenous mud. These velocities correspond to Δt_o values of 207 to 198 μs/ft. Lower values of Δt are probably more reasonable for nearly uncompacted high-porosity sediment.

In the case of the Uinta Basin, shales were deposited in a lacustrine environment during Green River Formation deposition and in an alluvial or overbank environment during later depositional periods. The value of interval transit time to use for muds deposited in an alluvial or overbank environment is not known. One could speculate that such muds initially have a somewhat higher velocity (low Δt_o) because of desiccation due to dry periods. However, it is likely that due to later burial a normal compaction trend similar to lacustrine or shallow marine environments will be obtained within depths of a few hundred feet. It is thus not likely that the value of Δt_o could reasonably be expected to vary much more than ± 10 μs/ft from 200 μs/ft. This translates to an uncertainty in Z_{OB} of about ± 152 m.

Many of the shale units used in the determinations of Z_{OB} came from the Uinta Formation, much of which formed in an alluvial environment. We calculated normal compaction trend slopes for units occurring only above the Green River Formation. The average slope was $b = 3.811 \times 10^{-5}$ ft^{-1} ($\sigma = 1.397 \times 10^{-5}$). This slope value leads to estimates of Z_{OB} which are generally about 300 m greater than those of Table 2. The uncertainty in this value of b is greater because of more variability in the data for shallower well depths. The net result of using the higher value of b, as is done in Table 2, is a possible underestimation of the overburden removed. Underestimating the overburden leads to lower values for maximum burial depths and consequent estimates of lower hydrocarbon maturity levels.

D. Burial History Model for the Basin

Once the amount of overburden removed at a particular well location is estimated, the value of Z_{OB} is added to the known present depth of a given marker horizon to obtain the maximum depth of burial for that marker. When this has been done for a series of marker layers, the burial history can be calculated by backstripping. To do this, we must know or estimate the porosity-depth function for the sediments. The function may have varying degrees of complexity depending on whether individual lithologic types such as sand, shale, and carbonate are treated separately or whether a single curve is used for the entire sediment pile. Bond and Kominz (1984) discuss various ways of constructing porosity curves.

It will be shown later that because of the kinetics of the Type I kerogen conversion process, temperatures of 120°C or more must be reached before significant conversion to hydrocarbons occurs. Thus, for the purposes of this study, detailed characterization of the early burial history is not necessary. For this reason we chose to use a simple porosity curve ($\phi = 0.35e^{-0.7z}$) covering the mid-range of the curves given by Bond and Kominz (1984, Fig. 2).

Detailed analysis of temperature data by Chapman et al. (1984) provides an estimate of 25°C/km for the present day geothermal gradient in the Uinta Basin. We here make the assumption that the geothermal gradient from the Tertiary to the present has been constant and ignore localized effects on thermal gradient such as overpressuring, lithologic variation and hydrothermal circulation. We choose a value of 10°C for the long-term average surface temperature. From these assumptions and the time-burial depth data corrected for compaction, we have constructed time-temperature-depth plots for the well locations of Table 2. A representative burial history and temperature is shown in Figure 7 along with values of heating rates for the base of the Eocene during the separate time intervals.

Figure 8 shows the effect of the uncertainty in removed overburden values on the heating rates and maximum temperature (T_{max}) attained. The initial burial history (prior to 41 My) is not sensitive to overburden estimates, but the later history is. A change of one standard deviation in the value of Z_{OB} results in 6°C - 8°C change in T_{max} and a change of about 0.1×10^{-9}°C/hr in the heating rate.

The effect of the type of density function used in the basin model is shown in Figure 9. The top curve is for the case where no compaction correction is made. Most of the differences in the curves occur during the early part of the basin history. The lower curve represents a compaction function similar to the maximum shale compaction curve of Bond and Kominz (1984, Fig. 2). It represents the extreme difference between early and late sediment volumes and would have the maximum effect on the burial curve. The middle curve, which is the compaction function used in this study, represents a mid-point between the two extremes. The net effect of the compaction function is nil on T_{max}, but the heating rate changes by about $\pm$ 0.1 x 10^{-9}°C/hr for the extreme cases.

To summarize, uncertainty in the value of Z_{OB} leads to an uncertainty of $\pm$ 8°C in T_{max} and an uncertainty of $\pm 0.1 \times 10^{-9}$ °C/hr in heating rate. Uncertainty in the porosity function has no effect on T_{max}, but leads to an uncertainty in the heating rate of 0.1×10^{-9} °C/hr. The geothermal

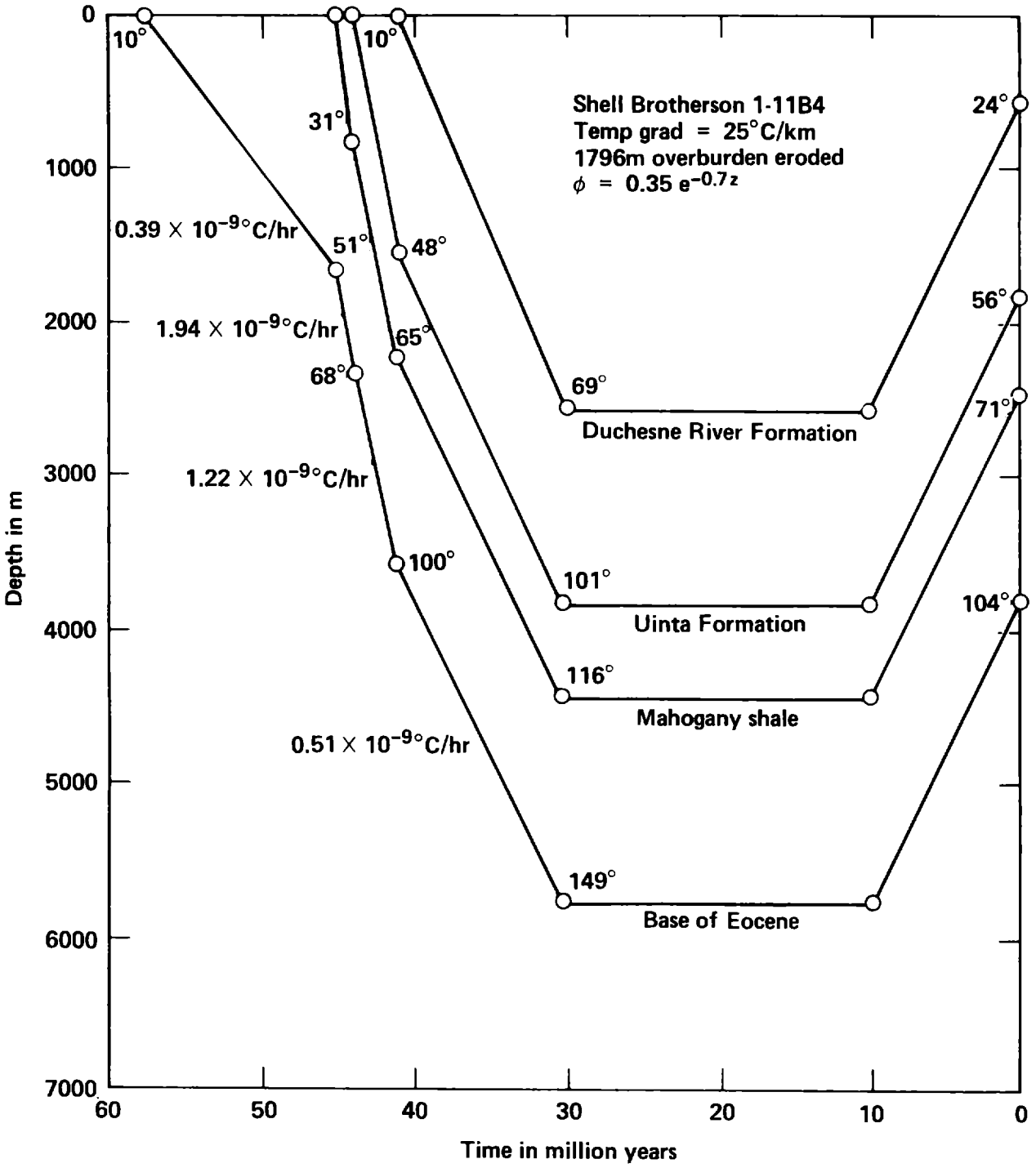

Figure 7: Burial history and temperature curve, corrected for compaction, for the Shell Brotherson 1-11B4 well.

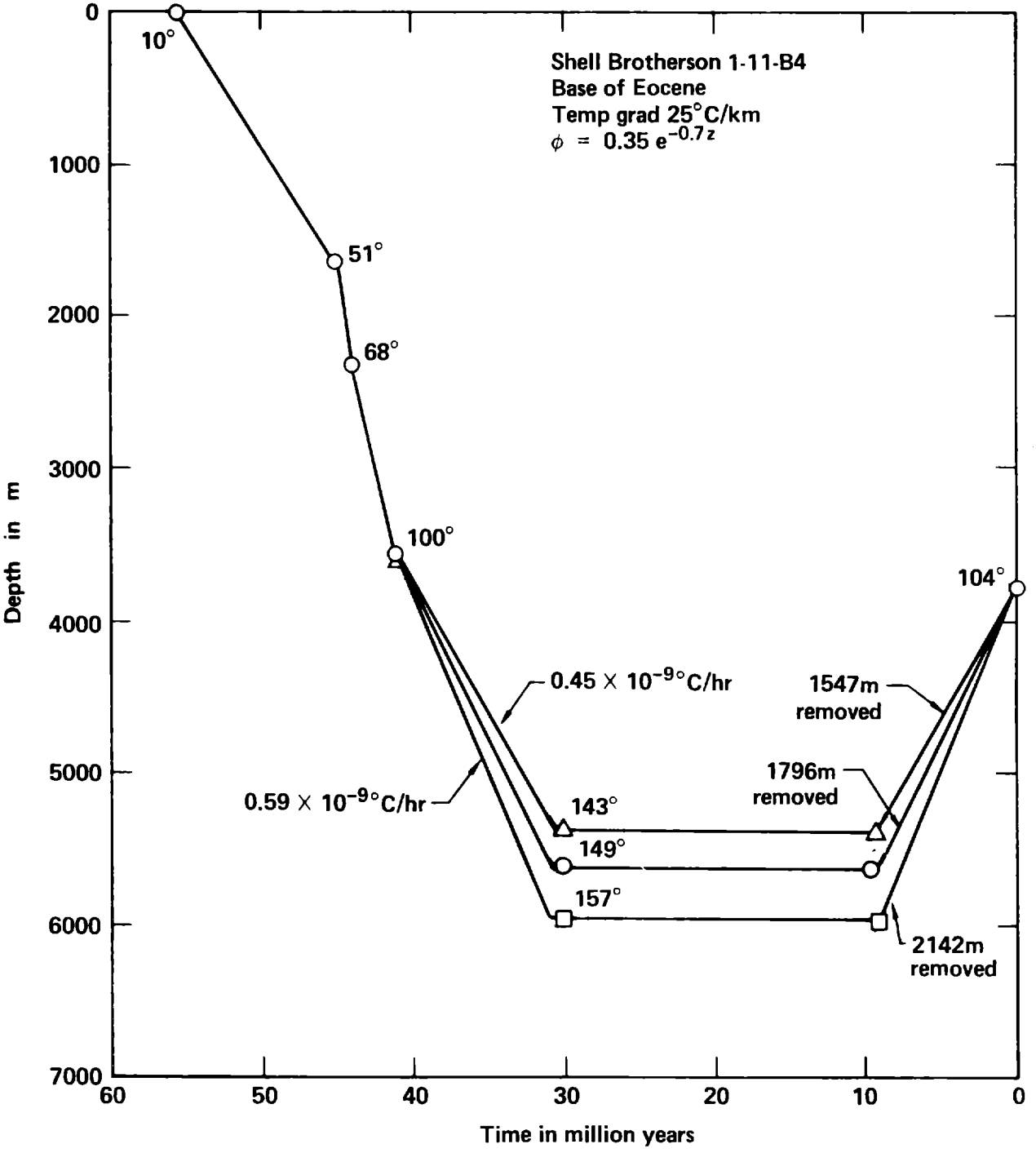

Figure 8: Burial history and temperature curve showing the effect of the value used for the amount of overburden removed. (Refer to Table 2).

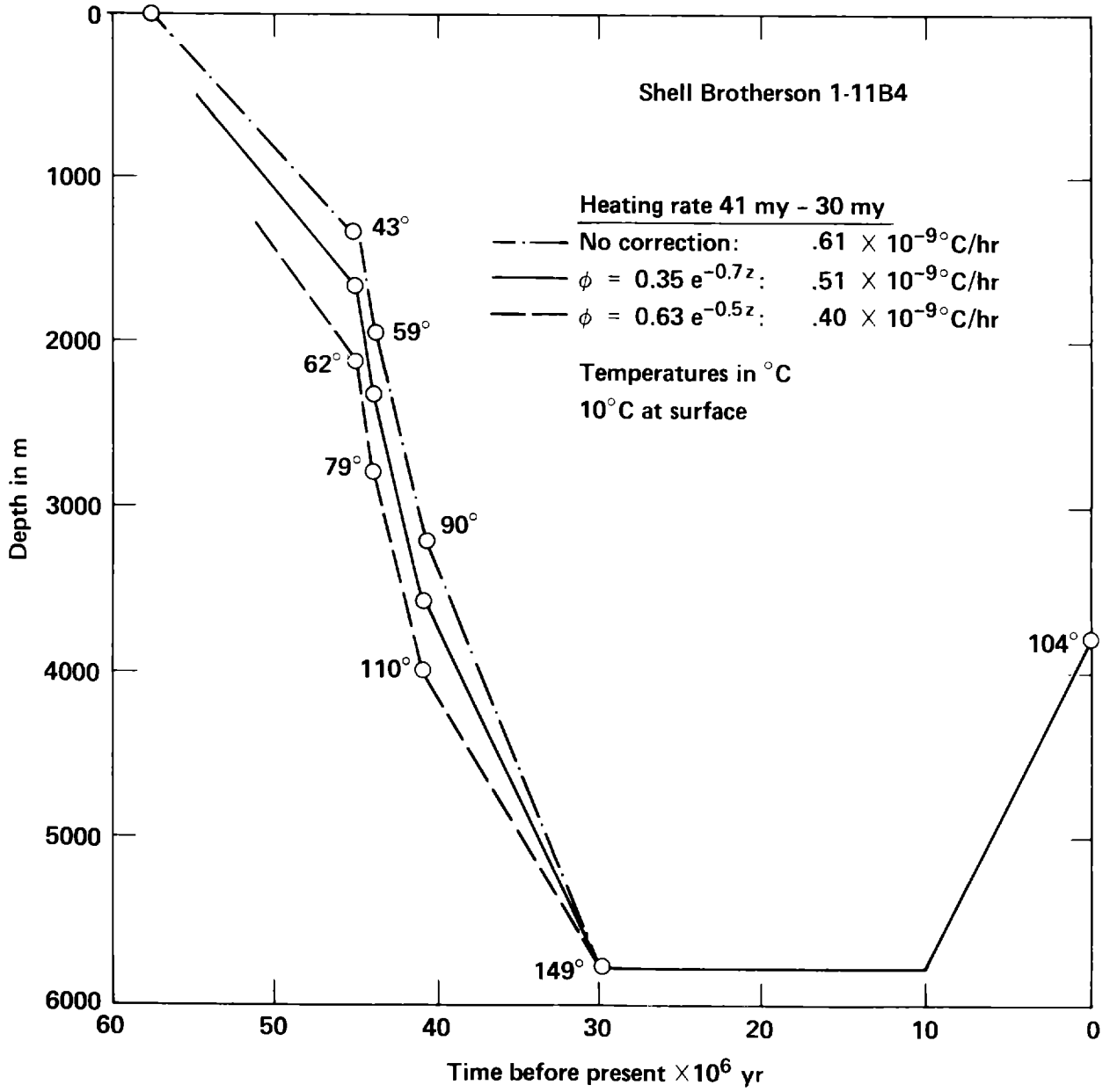

Figure 9: Burial history and temperature curve showing the effect of the value of the assumed porosity function.

gradient varies throughout the basin (Chapman et al., 1984) and the present-day gradient may be different from past gradients, thus its uncertainty is difficult to assess. Combining a ± 5°C/km uncertainty in geothermal gradient with a ± 300 m uncertainty in Z_{OB}, a net uncertainty in T_{max} of Fig. 7 of ± 35°C is obtained. This range of temperatures would certainly have a profound affect on hydrocarbon maturity; such differences can be evaluated by comparing the geologic model with hydrocarbon maturation data. It is shown below that the low uncertainty in the heating rate has an insignificant effect on hydrocarbon maturity calculations in comparison to the uncertainty in T_{max}.

The bulk of the Type I kerogen contained in post-Cretaceous rocks of the Uinta Basin occurs in the Green River Formation between the Mahogany shale and the base of the Eocene. This stratigraphic interval is of prime concern for hydrocarbon generation. Representative burial history and temperature curves for these Green River Formation units are shown in Figures 7, 10, 11, and 12.

Figures 7 and 10 are representative of the Altamont-Bluebell field where present-day burial depths are the greatest in the basin. The kerogen-bearing units have been heated to maximum temperatures of 149°C to 175°C. Maximum heating rates occurred during the period 41 to 30 My and range from 0.51 to 0.74×10^{-9}°C/hr. The maximum temperature attained by the base of the Eocene in the well from the Redwash field was much lower, 111°C, with a lower heating rate between 41 to 30 My of 0.16×10^{-9}°C/hr. Conditions at Pariette Bench were intermediate to the two other fields, with a maximum base Eocene temperature of 132°C and a heating rate of 0.35×10^{-9}°C/hr.

IV. Estimation of Kerogen Transformation

Although it has been known for many years that pyrolysis of kerogen yields liquid hydrocarbons, there has been some doubt about whether petroleum formation could be explained by a pyrolysis process. In the 1960's research established firmly that petroleum is formed predominantly by thermal transformation of kerogen (e.g., Philippi, 1965). Later, others tried to establish the time-temperature relationship for petroleum formation (e.g., Tissot et al., 1974; Tissot and Espitalie, 1975; Connan, 1974; Ishiwatari et

al., 1976; Waples, 1978). However, there is a persistent conflict between the 15-20 kcal/mole activation energies for kerogen conversion reactions determined from geological studies and the 40-60 kcal/mole activation energies determined from laboratory pyrolysis.

The rate of a first order chemical reaction is given by

$$dV/dt = -kt;\ k = A \exp(-E/RT) \tag{7}$$

where the variables are V: volume, t: time, E: activation energy, R: gas constant, T: absolute temperature, A: constant.

An analytical solution for a sample undergoing pyrolysis at a constant heating rate, H_r, is given by Van Heek and Juntgen (1968):

$$\frac{dV}{dt} = AV_\infty \exp\left[-\frac{E}{RT} - \frac{A}{H_r}\int_0^T \exp(-\frac{E}{RT})\, dT\right] \tag{8a}$$

$$\simeq AV_\infty \exp\left[-\frac{E}{RT} - \frac{ART^2}{H_r E}\exp(-\frac{E}{RT})\right] \tag{8b}$$

Campbell et al., (1978) used this expression to determine an accurate rate expression for the generation of oil from Green River oil shale:

$$k(s^{-1}) = 2.8 \times 10^{13}\, e^{-26390/T} \tag{9}$$

The exponential factor corresponds to an activation energy of 52.4 kcal/mole. Campbell et al. (1978b) and Burnham and Singleton (1983) have verified the accuracy of Eq. (9) down to 2°C/hr and 1°C/hr, respectively. Moreover, Saxby and Riley (1984) report that torbanite heated at 1°C/week produces most of its oil between 250°C and 300°C. Eq. (9) predicts a maximum rate of oil generation at 291°C.

Since the geological heating rate is often approximately constant during the oil generation phase, we can use Eq. 8 and 9 for an initial estimate of the relationship between laboratory pyrolysis experiments and the geological parameters developed in the preceding sections.

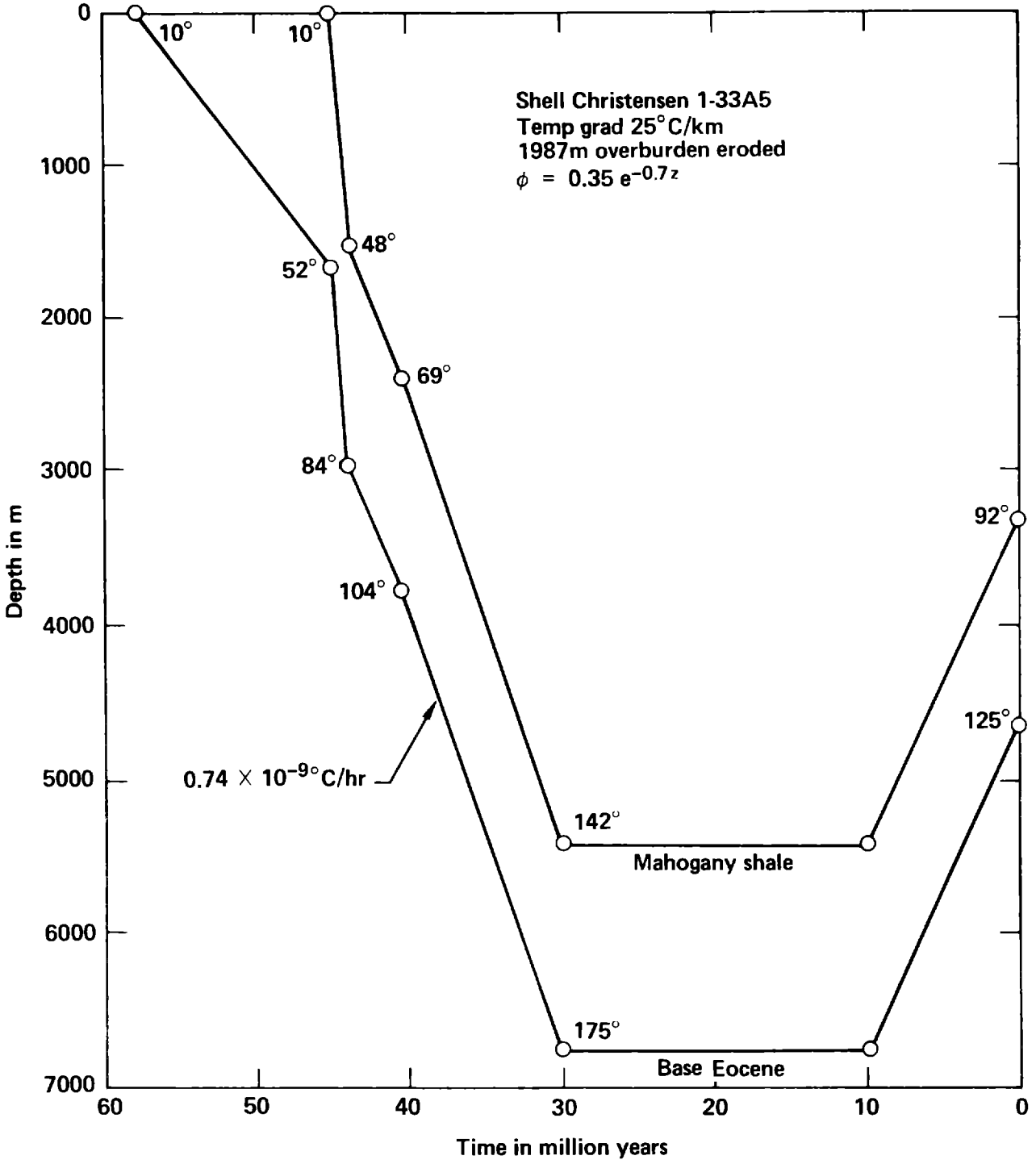

Figure 10: Burial history and temperature curves for the Green River Formation at the Shell Christensen well in the Altamont-Bluebell oil field.

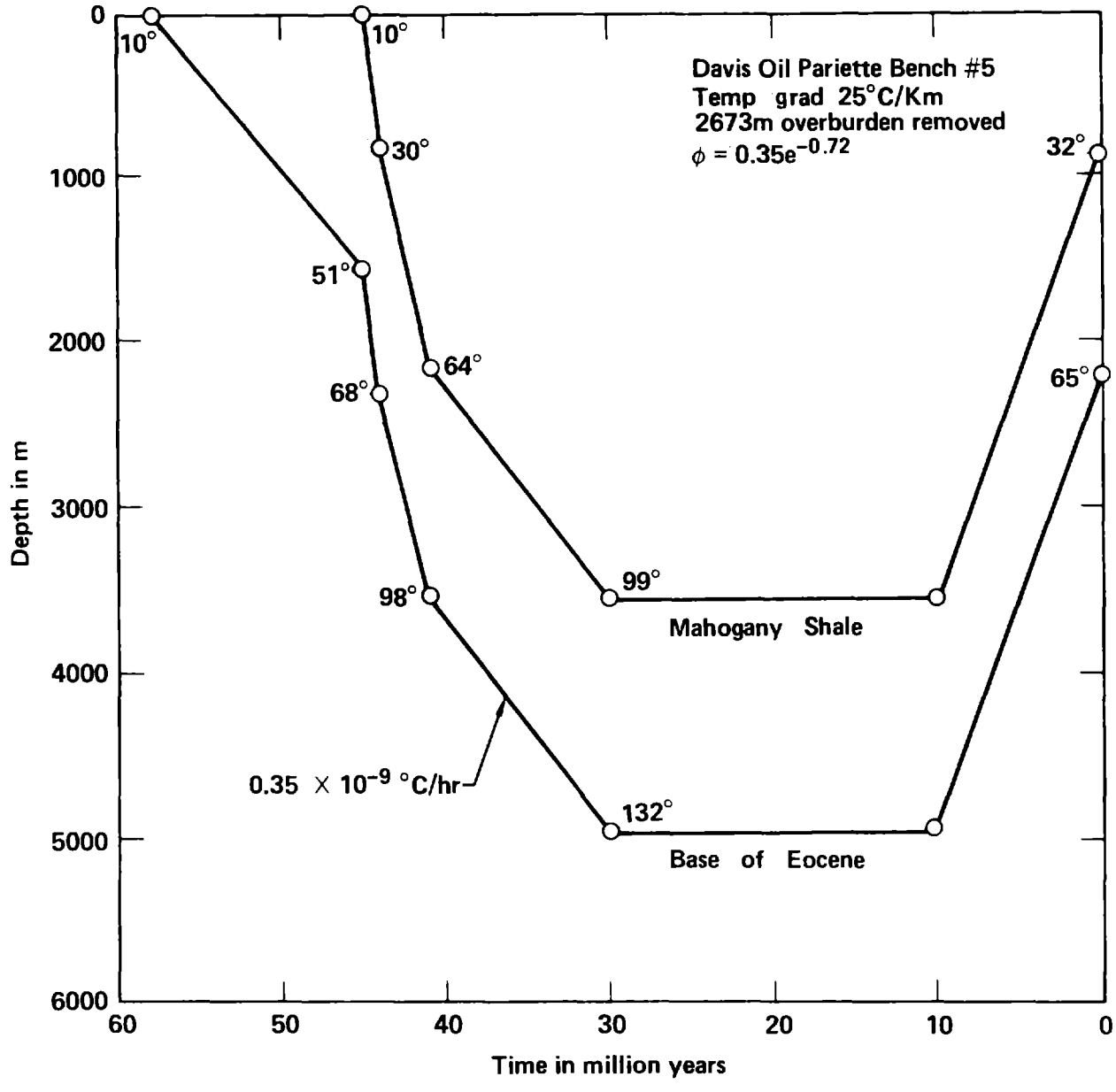

Figure 11: Burial history and temperature curves for the Green River Formation at the Davis Oil Pariette Bench well.

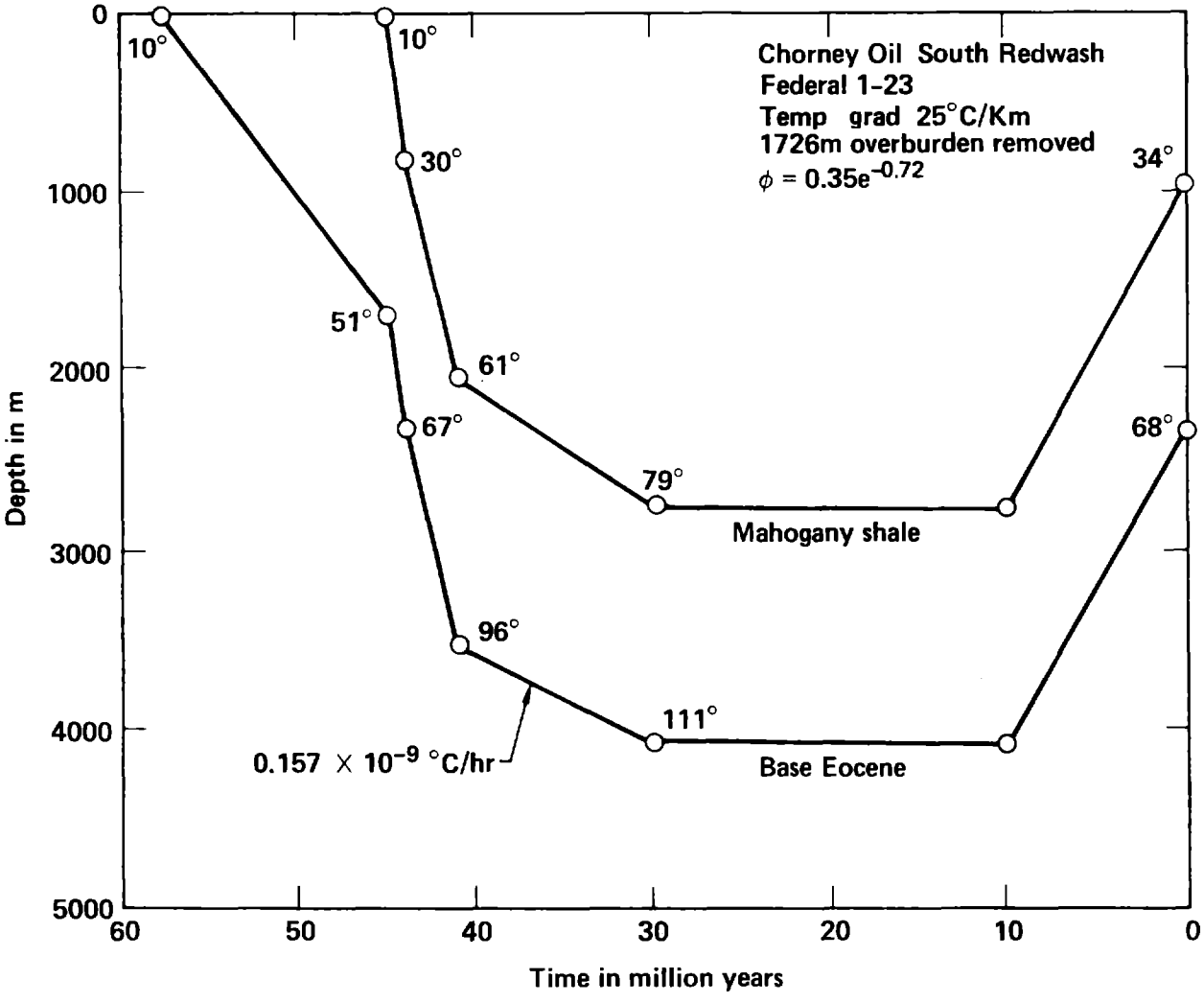

Figure 12: Burial history and temperature curves for the Green River Formation at the Chorney Oil South Redwash well in Redwash oil field.

This nonisothermal method to simulate the macroscopic conversion of Type I kerogen to petroleum at various heating rates has been used to generate the curves of Figure 13. In the calculations, we used heating rates that are the same order of magnitude as geologic rates estimated for the Uinta Basin. For a heating rate of 10^{-8} °C/hr the temperature of the peak rate of oil production, T_p, is 170°C, while T_p is only 139°C for a heating rate of 10^{-10} °C/hr. A change of 10% in the heating rate changes T_p by less than 1°C. The values of T_p shown are close to the values estimated for the maximum temperatures attained in the Uinta Basin, indicating that a potential for oil generation is present and that values used for Z_{OB} and the geothermal gradient are approximately correct.

The extrapolation from laboratory to geological conditions is more sensitive to the value of activation energy used than to the value of the rate at laboratory conditions. Doubling the rate at all temperatures by doubling the preexponential factor (Eq.9) causes T_p at 0.5×10^{-9} °C/hr to decrease only from 149°C to 145°C. However, in the laboratory case, this change causes T_p at 2°C/min to shift from 433°C to 421°C, which is outside the range of experimental error. In contrast, if the activation energy is decreased by 4.7 kcal/mole and the preexponential factor is adjusted so that T_p at 2°C/min remains at 433°C (this, in fact, corresponds to the results of Shih and Sohn (1980)), T_p at 0.5×10^{-9} °C/hr decreases from 149°C to 134°C. This second case describes the approximate uncertainty in activation energy for the geological extrapolation. Use of a significantly lower activation energy, such as the 15-20 kcal/mole corresponding to the "rate doubling every 10°C" rule (Waples, 1980), results in an unrealistic extrapolation. Such low apparent activation energies are an artifact of either diffusion controlled reactions or a distribution of higher activation energies.

Figs. 7, 10, 11, and 12 show that prior to 41 My ago there was very little potential for oil generation because temperatures of the Green River Formation never exceeded 100°C. Even at low heating rates Fig. 13 shows that temperature must exceed 120°C in order to get any oil production. Heating rate and temperature attained during the time period of 41 to 30 My is the key

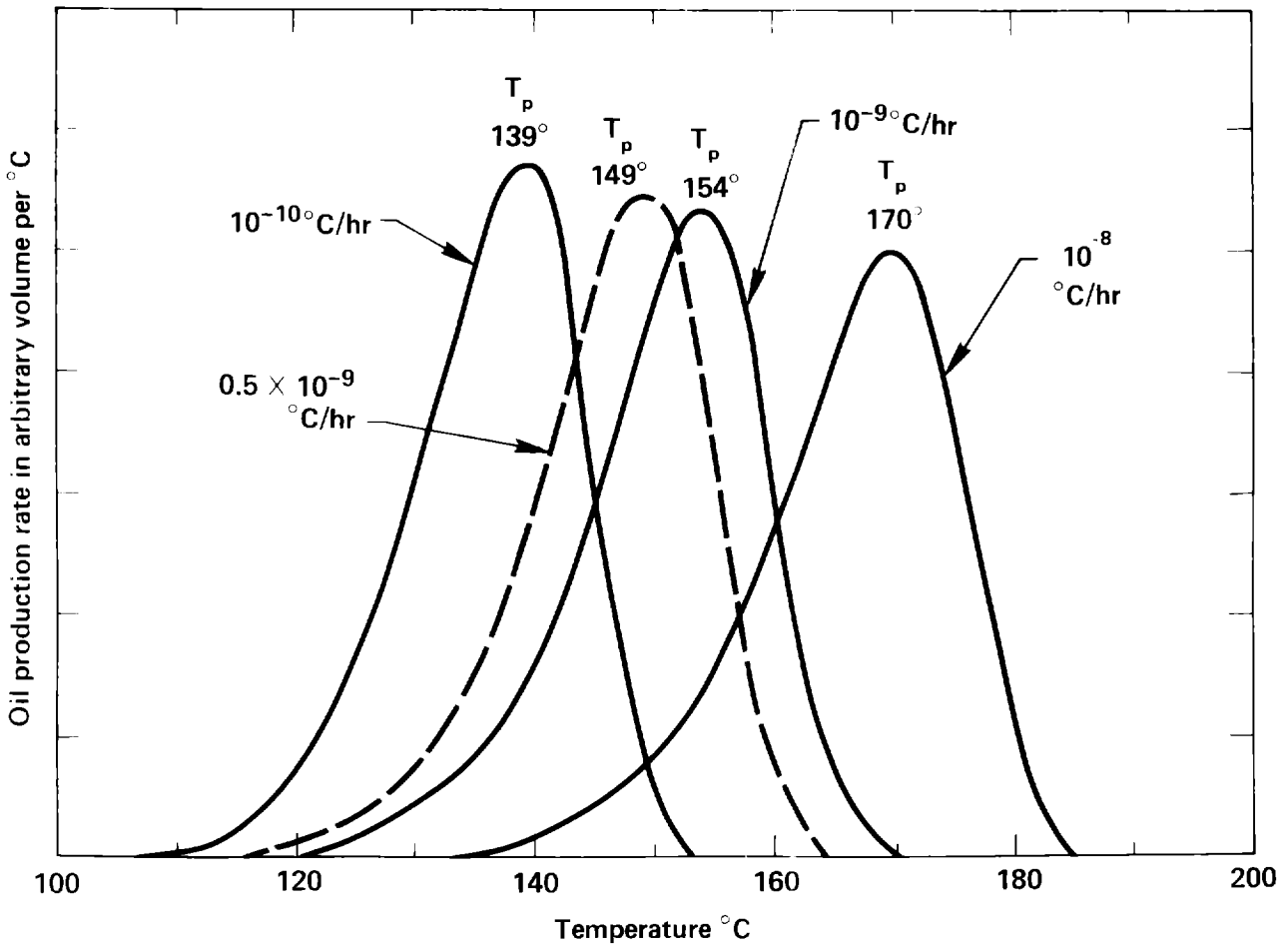

Figure 13: Oil production rate curves for the conversion of Type I kerogen using the results of Campbell et al. (1978). T_P is the temperature corresponding to the maximum rate of oil production. Slower heating rates lead to lower values of T_P.

to the analysis. The Shell Brotherson and Shell Christensen wells (Figs 7 and 10) are well within the oil production "window" because, at the heating rates shown, maximum oil production occurs between 149°C and 154°C. Kerogen in the Shell Christensen well would be expected to be much more mature than that of the Shell Brotherson well. Temperatures and heating rates estimated for the Davis Oil Pariette Bench well indicate that the conversion level is well below peak production according to Figure 13. Using values of 915 m or less for Z_{OB} at Pariette Bench as suggested by Pitman et al. (1982), would put the level even lower. In the same way it is seen that the Chorney Oil S. Redwash well (Fig. 12) shows temperatures much too low to be in the oil production "window." The fact that oil is found in the Pariette and Redwash areas suggests that (assuming our modeling is correct) generation occurs at greater depths, significant vertical or lateral migration of oil has taken place, or both.

In Figures 14 and 15 show oil generation curves based on heating rates calculated from the geologic basin model. In each case the oil-generation curves are superimposed on a lithologic and oil production log for the well as drilled. The wells are close together in the Altamont oil field and temperatures of the base of the Eocene are estimated to have reached 149°C to 153°C by 30 My ago. The peak of the oil-generation curve in each case closely corresponds to the depths of oil shows or recovery. This indicates that the higher value of activation energy used in the calculations is applicable to the petroleum formation process. The maximum oil-recovery depth of Fig. 15 is about 300 m above the depth of the maximum calculated oil generation. This may indicate that temperatures attained by units in the well have been overestimated by 10°C or so. The shape of the shaded area indicating overpressuring in the wells corresponds to the rise of the oil generation curve. This supports the theory that overpressuring in this area may be caused by volume changes accompanying oil and gas generation.

These preliminary results are encouraging. They indicate that the geologic model is reasonable and consistent with extrapolations of simple laboratory retort models of kerogen evolution. In contrast, the parallel reaction scheme of Tissot and Espitalie (1975) predicts multiple oil generation peaks (Fig. 16) at both laboratory and geological heating rates

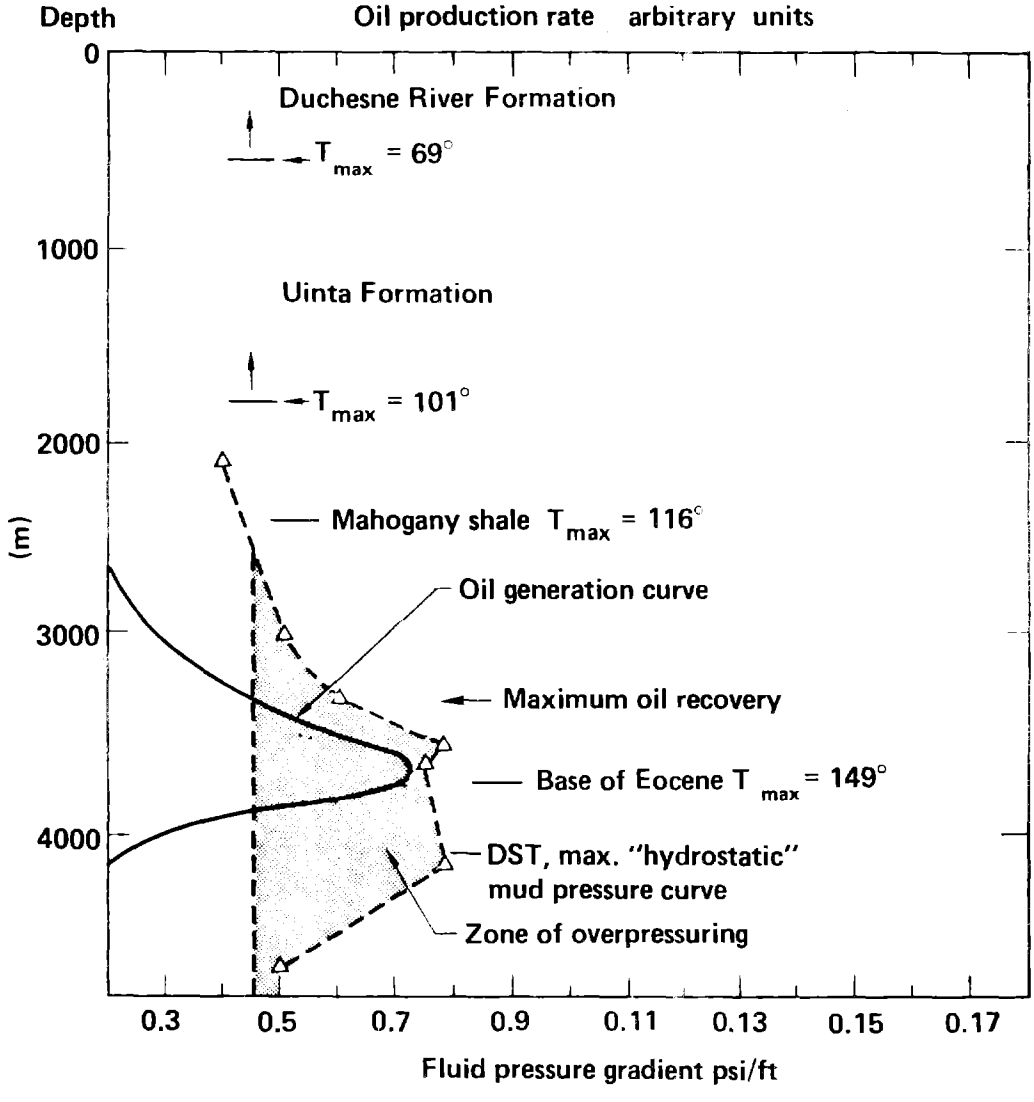

Figure 14: An oil generation curve for Shell Brotherson 1-11B4 well (location 2S, 4W) superimposed on the lithologic log showing oil production depths and pore fluid pressure data. The oil-generation curve is based on heating rates determined from Fig. 7. Data from Meissner (1982) and Fouch (1981).

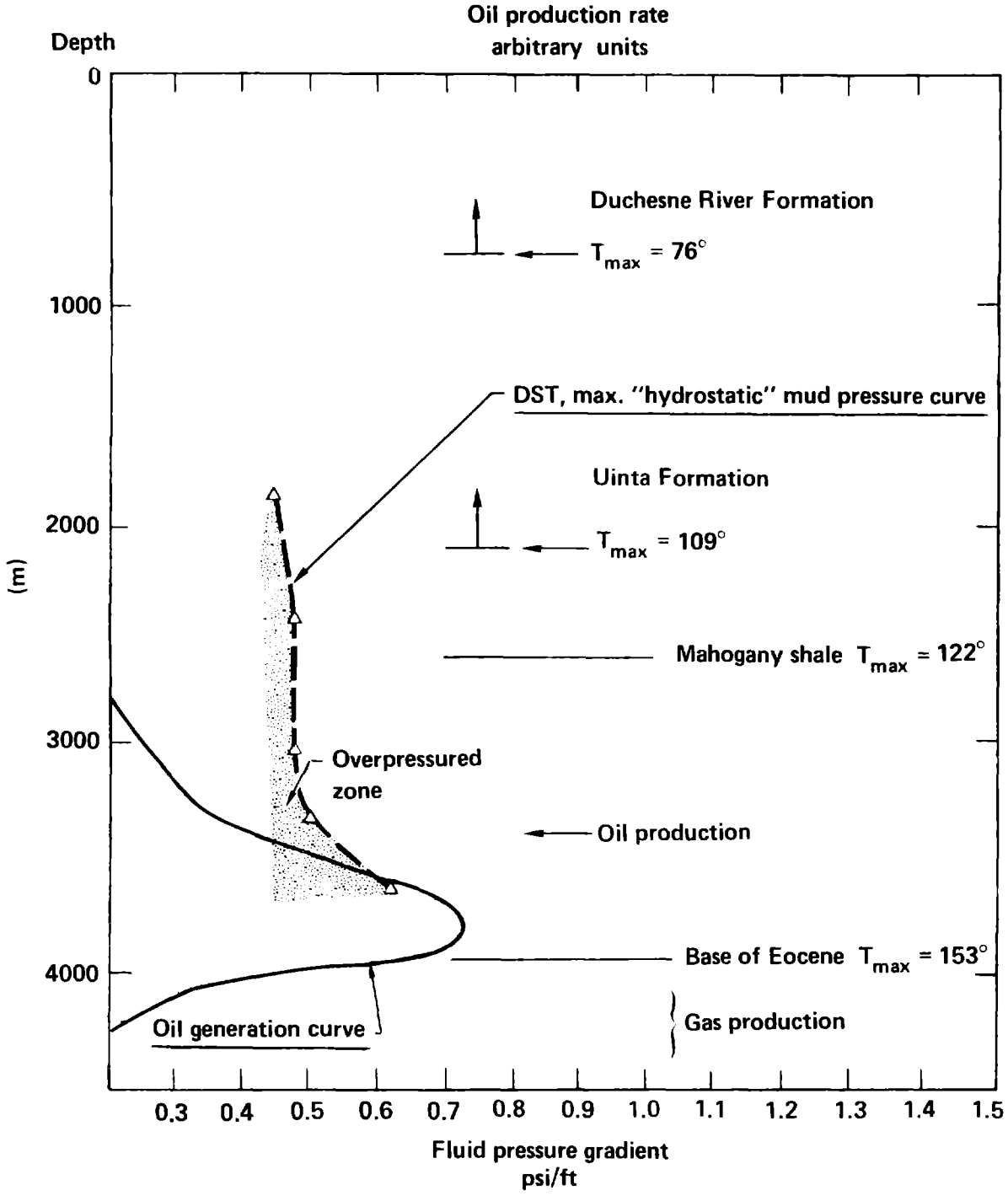

Figure 15: Oil generation curve for Shell Miles #1 well (location 1S, 4W) superimposed on the lithologic log showing oil production depths and pore fluid pressure data. The oil generation curve is based on heating rates determined from the basin model. Other data from Meissner (1982) and Fouch (1981).

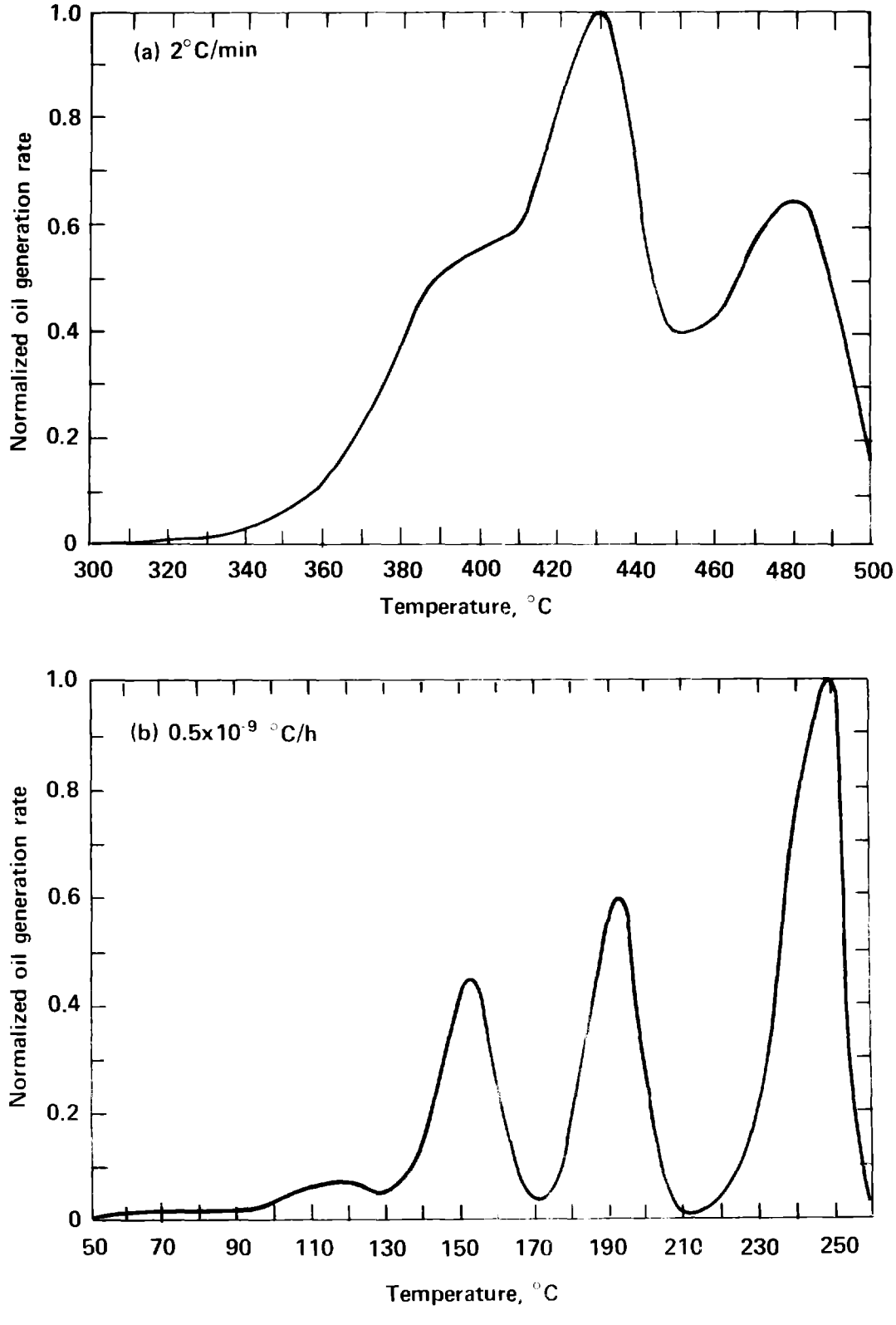

Figure 16. Normalized rate of oil generation calculated using the kinetic parameters of Tissot and Espitalie (1975) in Eq. 7b. The multiple peaks come from their assumption of six parallel oil-generating reactions.

even though only one is observed. Next, we employ a more detailed geochemical model and predict hydrocarbon compositions as well as generation rates. We then compare the modeled composition and generation rate data with published data for the oil fields.

V. Formulation of a Detailed Geochemical Model

While the rate of kerogen decomposition is central to understanding the origin of petroleum, many other reactions are also important. Figure 17 shows that continued heating can convert oil to gas if the oil does not migrate to a cooler reservoir. Secondary reactions are also important in oil shale processing. We have recently combined our understanding of the organic pyrolysis reactions into a detailed chemical model (Burnham and Braun, 1985), which is summarized in Table 3. The model accurately calculates amounts and rates of oil and gas formed under wide range of pyrolysis conditions. It consists of 67 first-order, nonlinear, ordinary differential equations solved by numerical integration. (Numerical integration removes the constant heating rate restriction of Eq. 7.) The equations specify the rate of change of each gas, liquid, and solid component in terms of the vaporization or chemical reactions. The generated oil is divided into 50°C boiling-point interval fractions, allowing (for laboratory experiments) a direct calculation of liquid-phase residence time prior to evaporation. For the geological case oil evaporation is not included (to conserve computer time), but this feature allows us to calculate variations in distillation characteristics of the oil with thermal history. The initial oil generated is heavier than is normally produced, so this formalism automatically includes the pyrobitumen intermediate of some models. In the original model we incorporated a kinetic expression that could calculate the dependence of mineral dehydration on pressure and heating rate (Burnham and Braun, 1985). However, this part of the model was eliminated for these calculations because we thought it was too empirical to extrapolate to geological conditions.

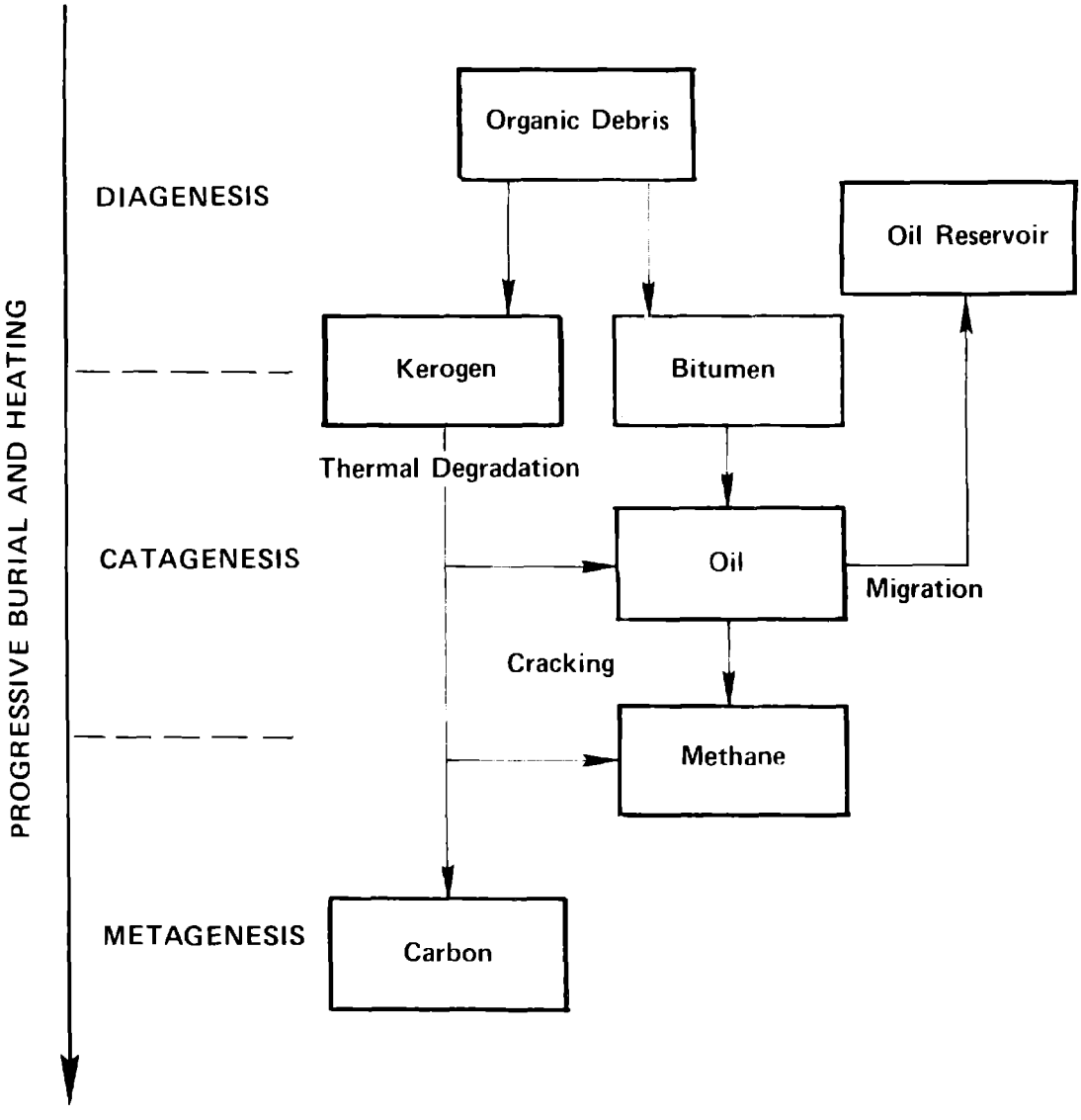

Figure 17. Diagram illustrating the mechanism of petroleum formation. The conversion of kerogen to oil to methane is actually a continuum process.

Table 3. Chemical reactions and rate expressions that define the model. For a detailed explanation of the model and parameters see Burnham and Braun (1985).

Reaction	Rate Expression[a]
Kerogen pyrolysis & bitumen	
$100CH_{1.50}N_{0.025}O_{0.05} \rightarrow 5.3CH_{1.56}N_{0.021}O_{0.01}$	Initial oil (bitumen)
$+ 74.2CH_{1.56}N_{0.021}O_{0.01}$	5% by $k_b = 7\times10^{13}e^{-26390/T}$
$+ 14.7CH_{0.63}N_{0.056}O_{0.02}$	95% by $k_o = 2.8\times10^{13}e^{-26390/T}$
$+ 0.3CO + 1.0H_2O$	k_o = above
$+ 0.6CH_4$	$k_x = 9\times10^{12}e^{-26390/T}$
$+ 3.6CH_x$	
$+ 1.0H_2$	$k_h = 5\times10^{12}e^{-26390/T}$
$+ 1.3CO_2$	$\frac{1}{3}$ by $k_1 = 1\times10^{13}e^{-(22000\pm2200)/T}$
	$\frac{2}{3}$ by $k_2 = 7\times10^{13}e^{-(26390\pm1800)/T}$
Oil coking	
$100CH_{0.99}N_{0.038}O_{0.02} \rightarrow 95CH_{0.63}N_{0.04}O_{0.02}$	$k_\ell = \dfrac{3.2\times10^{10}e^{-17620/T}}{(1 + 2\times10^{-4}P_{H_2})}$
$+ 3CH_4 + 11H_2 + 2CH_x$	
Oil cracking	
$Oil_i \rightarrow Oil_{j<i} + char + gases$	$k_{c,i} = A_i \cdot 2.11\times10^{10}e^{-26390/T}$
Secondary char pyrolysis	
$100CH_{0.63}N_{0.05}O_{0.02} \rightarrow 94.5CH_{0.23}N_{0.03}O_{0.02}$	$k_s = 3.3\times10^{9}e^{-(23210\pm2285)/T}$
$+ 5.5CH_4 + 6.4H_2 + (2.2NH_3)$	
Tertiary char pyrolysis	
$100CH_{0.23}N_{0.03}O_{0.02} \rightarrow 100CH_{\sim0.1}N_{0.03}O_{0.02} + 8.0H_2$	$k_t = 3.1\times10^{13}e^{-(39000\pm4090)/T}$
Dolomite decomposition	
$MgCa(CO_3)_2 \rightarrow MgO + CaCO_3 + CO_2$	$k_d = 2.5\times10^{10}e^{-29090/T}$

[a] First-order reaction unless otherwise noted. Activation energies with ± values use distributed activation energy theory. All rate constants in s^{-1} and pressures in Pa.

The model includes rate expressions for gas formation, both during the original kerogen decomposition and from secondary pyrolysis of the carbonaceous residue. The original analysis by Campbell et al. (1980) showed that it was necessary to use a gaussian distribution of activation energies (Anthony and Howard, 1976) for hydrogen and methane generation from char. We adopted a similar form for CO_2 generation from kerogen. Preliminary calculations showed that lower activation energies of Campbell, which were used previously for gas generation from kerogen (Burnham and Braun, 1985), result in gas generation proceeding oil generation by 20°C at geological heating rates. We believe that this is chemically unreasonable and results from slight errors in the measurements, so we adopted the same activation energy for all kerogen pyrolysis reactions and adjusted the preexponential factors so that T_p for each component was unchanged at 2°C/min.

Oil can be destroyed by both coking and cracking. Oil coking is the polymerization and condensation of oil components, usually hetero-aromatics to form predominately a solid residue (coke). It leads to an increase in aliphatic content and a decrease of the heteratom content. In contrast, oil cracking is the fission of aliphatic structures to smaller molecules, ultimately methane. It leads to a concentration of aromatic component in the oil. There is, of course, overlap between the types of reactions, but this separation has proved useful. Correlations have been developed for the dependence of oil density and elemental composition on the amount of coking and cracking (Stout et al., 1976; Burnham, 1981; Burnham and Singleton, 1983), but they have not yet been incorporated into the model.

A few general features of the model are worth noting. Figure 18 shows the rate of gas generation from the various sources. Note that the temperature of the maximum rate of gas generation in the absence of oil cracking trails the oil generation by about 5°C. Oil cracking produces another peak in gas generation at a temperature about 40°C higher, although the peak would be smaller if oil migration occurred. These additional gas generation processes may be responsible for the persistence of the overpressurized zone shown in Figure 14.

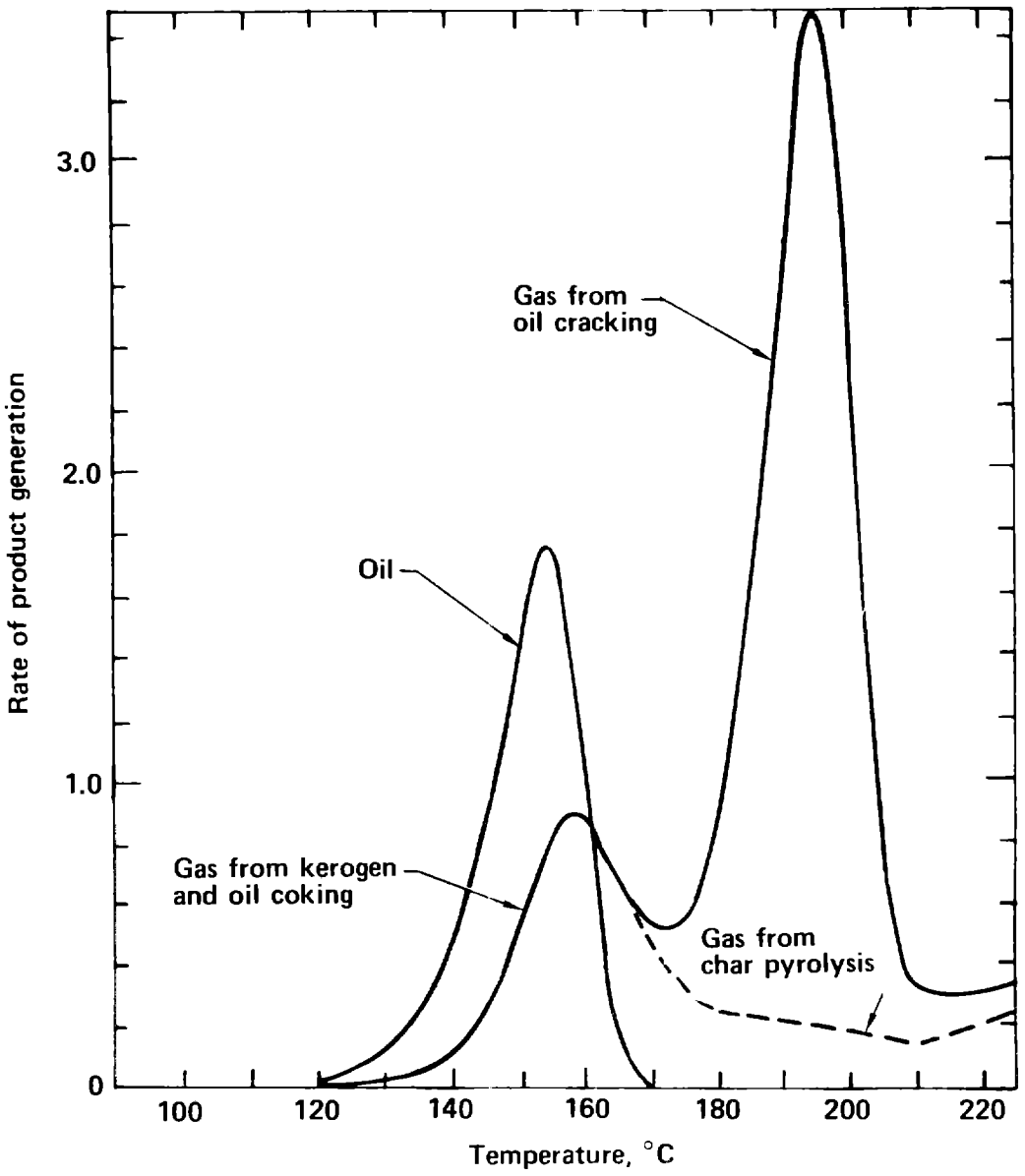

Figure 18. Rates of oil (10^{-15} kg/kg-s) and gas (10^{-15} mole/kg-s) generation at a heating rate of 1.2×10^{-9} °C/hr. The amount of gas produced from oil cracking depends on how much oil does not migrate.

A variety of gas-generating processes cause the gas composition to change during the course of maturation. Figure 19 shows one common indicator, C_2-C_4/C_1-C_4 in the gas. With oil cracking, this ratio increases during oil generation and reaches a maximum at the completion of oil generation. At higher temperatures, methane generation from char pyrolysis causes the ratio to decrease. If oil remains to be cracked, the ratio increases further. The present version of the model does not allow C_2-C_4 hydrocarbons to crack further to methane, so this ratio may be too high at very high maturation. Likewise, the model generates substantial quantities of hydrogen which react, at high pressures and slow heating rates, to form methane and hydrogenated oil. Future work will address these weaknesses.

We cannot at present vary pressure with time in the model calculations. The main effect of pressure is on the rate expression, which affects rates and composition of the products of cracking (Burnham and Braun, 1985). Higher pressure inhibits cracking and results in less gas formation for a given amount of cracking. Pressures representative of averages during the high temperature intervals (maximum burial portion) were estimated from curves given by Narr and Currie (1982), which account for overpressuring. These average pressures were estimated to range from 40 MPa to 90 MPa and kept as a constant throughout each run.

Numerous studies have shown that the composition of the early oil is substantially different from the remainder. Coburn and Campbell (1977) and Burnham et al. (1982) have shown that most of the biological-marker compounds are evolved in the first 10 to 20% of the oil. Some of these compounds are in the bitumen (initial oil) and some are released by kerogen decomposition. Figures 20 and 21 show conversion-dependent oil-composition indicators that we calculated using data of Coburn and Campbell (1977) and Burnham et al. (1982).

To mimic the characteristic evolution of marker compounds, the detailed model has an initial oil content made up from to 5% of the original organic matter. We allow 5% of the kerogen decompose by a faster rate constant. We found that we did not have to use a Gaussian distribution of activation energies for the early oil to make the change in oil-composition indicators,

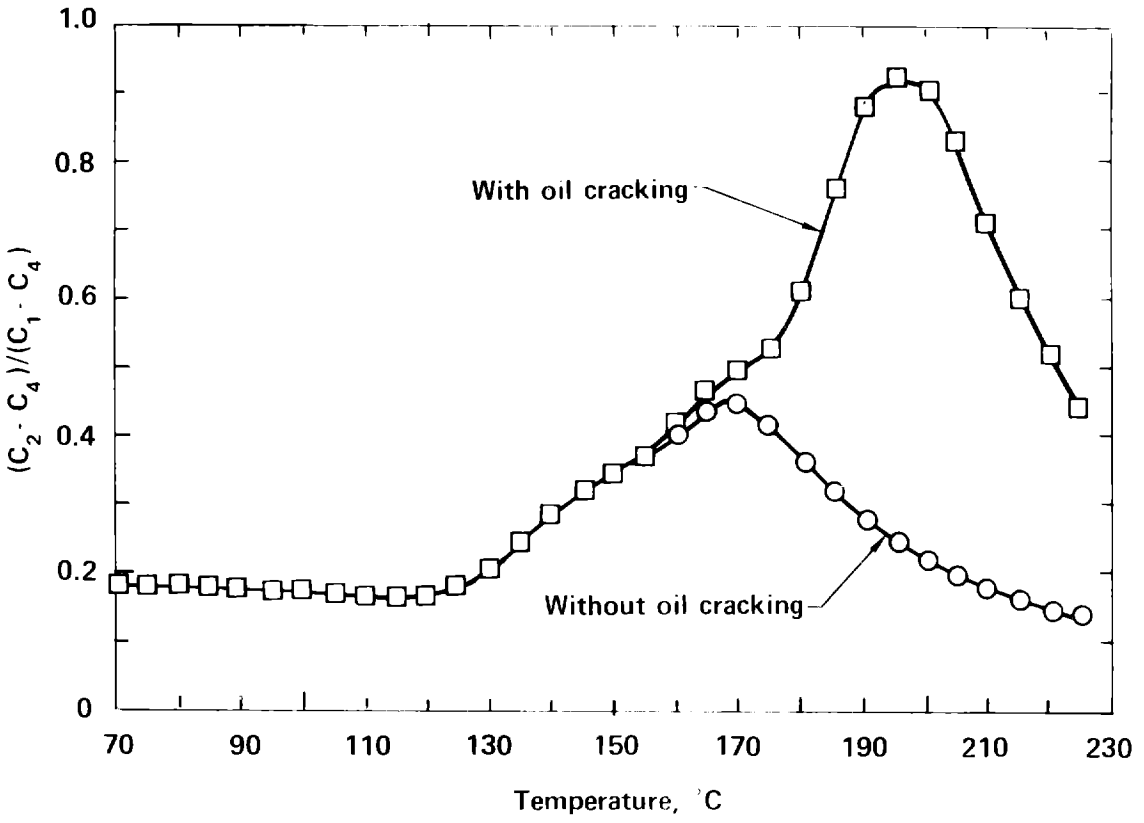

Figure 19. Changes in the ratio $(C_2 - C_4)/(C_1 - C_4)$ with temperature for the cases with and without oil cracking.

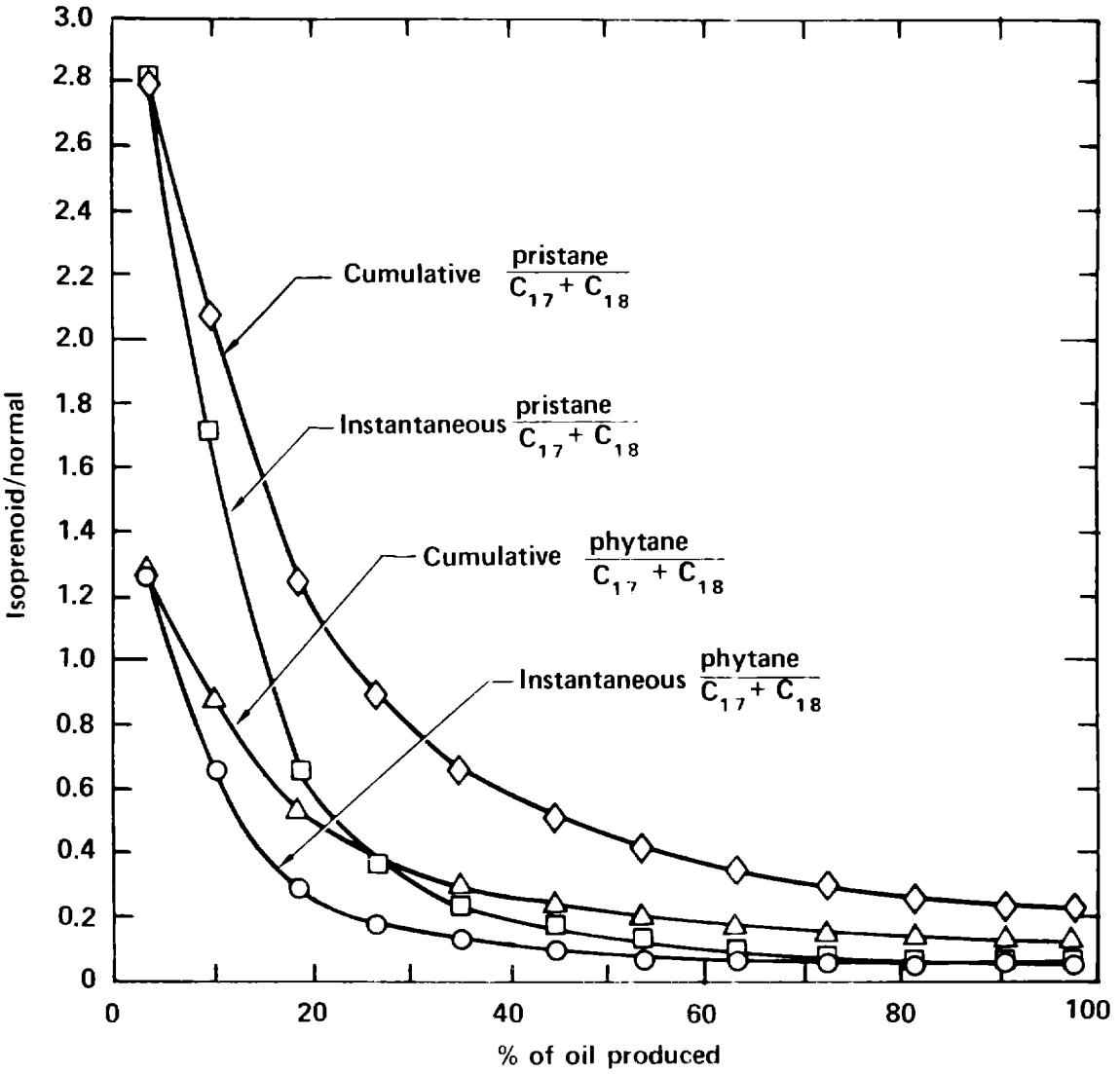

Figure 20. Maturity indicators calibrated to percent oil produced.

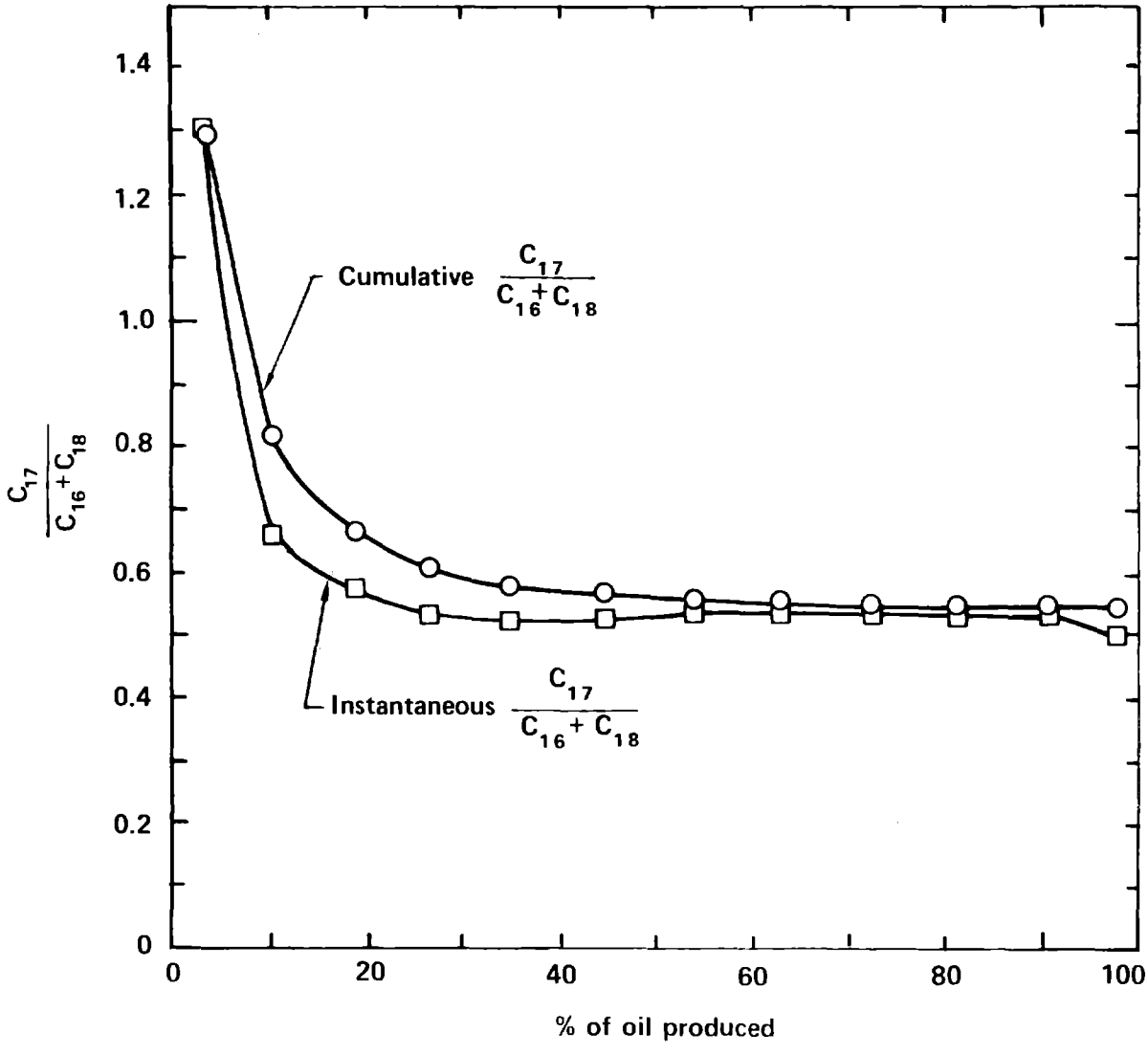

Figure 21. Calibration of $C_{17}/(C_{16} + C_{18})$ with percent oil produced.

through the course of kerogen pyrolysis, agree with oil composition data. The model does not calculate oil composition explicitly, but it does calculate qualitative oil composition indicators based on the amount of the kerogen types remaining and their current rate of decomposition. The first indicator (integral indicator of oil composition, I.O.C.) is equal to the the sum of the mass of bitumen plus the oil generated by the faster rate constant, divided by the total mass of oil (including bitumen). If we assume that biological markers from kerogen are generated at the faster rate, the I.O.C. should be proportional to the branched plus cyclic content of the oil in the absence of migration. The second indicator (differential indicator of compositiion, D.O.C.) is equal to the rate of oil generation by the faster rate constant divided by the total oil-generation rate. If oil migration were instantaneous, this indicator would be proportional to the branched plus cyclic content of the oil. The dependence of these indicators on the extent of kerogen conversion is given in Figure 22. The calculated D.O.C. has a lower initial change than the differential curves in Figures 20 and 21 because they contain a contribution from initial bitumen.

VI. Application of the Detailed Geochemical Model

We ran the model, with heating rate and temperature data from several wells, to calculate oil formation and degradation at various depths. Table 4 summarizes the results for several of the wells listed in Table 2. The conversion of kerogen ranges from 7 to 100%. The elemental composition of the solid remaining in the oil, plotted in Figure 23, indicates that the material follows, as expected, the maturation curve of Type I kerogen shown by Tissot et al. (1978). The boiling point distribution of the liquid oil for several selected samples is shown in Figure 24. The oil becomes noticeably lighter with increasing maturity. This is due to three effects: the oil generated from kerogen is lighter than the original bitumen, coking tends to remove heavier oil components, and cracking converts heavy components to light ones. An interesting observation is that essentially all the generated cokable oil (30% of the total) has coked. This accounts, in part, for the difference in aliphatic content of petroleum and most laboratory pyrolysates. Another observation is that although very little of the oil has cracked to gas, very few high boiling point components remain in two of the oil samples. For the

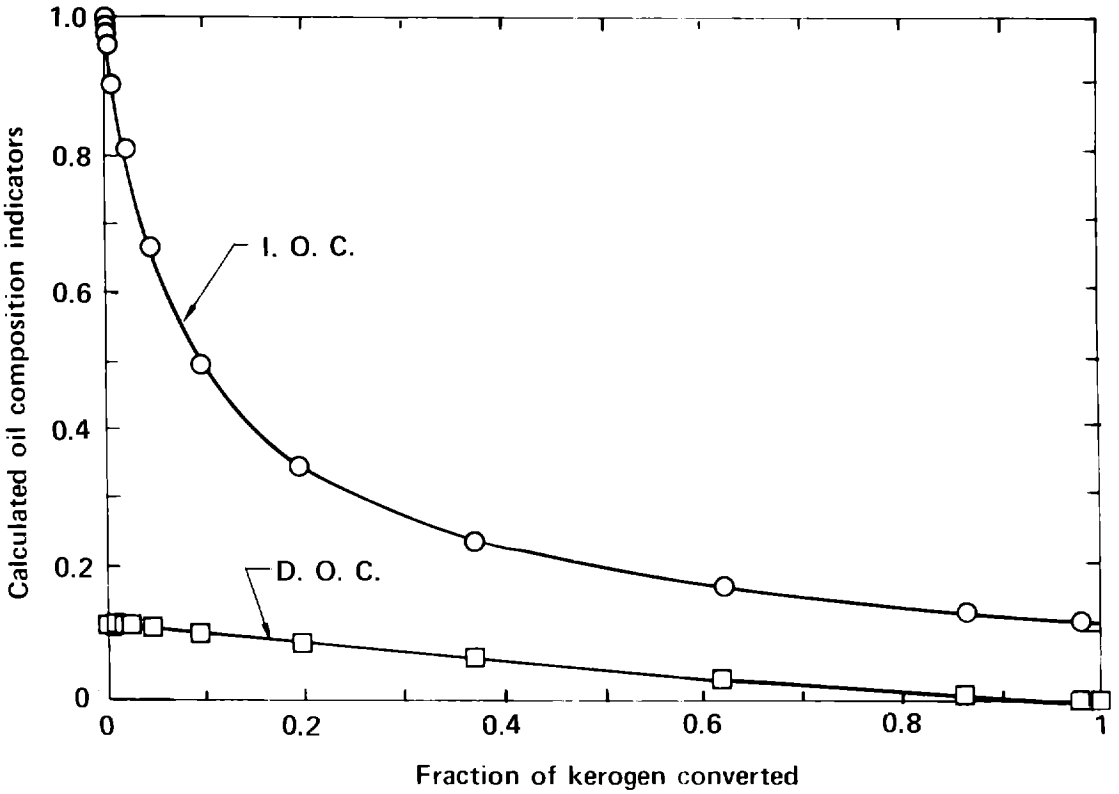

Figure 22. Calculated maturity indicators (I.O.C.-integral oil composition, D.O.C.-differential oil composition) plotted as a function of the fraction of kerogen that has been converted.

Table 4. Calculated compositional fractions for selected depths in particular wells. Input data came from Figs. 7, 10, 11 and 12 and similar determinations.

Well Name	Depth* (m)	T_{max} (°C)	H/C	O/C	Oil Ungen-erated	Oil Coked	Oil Cracked	Liquid Oil	I.O.C.	D.O.C.
1.Energy Res. Gp. Broadhurst #13	1435	91	1.48	0.044	0.933	0.022	0.00	0.045	0.99	0.12
2.Energy Res. Gp. Broadhurst #13	1756	99	1.48	0.042	0.930	0.023	0.00	0.048	0.96	0.12
3.Davis Oil Pariette Bench #5	927	100	1.48	0.042	0.930	0.023	0.00	0.047	0.95	0.12
4.Shell Brotherson 1-11B4	2003	105	1.47	0.041	0.925	0.024	0.00	0.051	0.89	0.11
5.Shell Brotherson 1-11B4	2643	121	1.42	0.037	0.787	0.066	0.00	0.147	0.38	0.09
6.Energy Res. Gp. Broadhurst #13	2758	124	1.39	0.036	0.670	0.101	0.00	0.229	0.29	0.08
7.Davis Oil Pariette Bench #5	2246	133	1.07	0.034	0.271	0.220	0.00	0.506	0.15	0.02
8.Shell Brotherson 1-11B4	3164	134	1.02	0.034	0.225	0.234	0.003	0.538	0.14	0.01
9.Gulf Duchesne Co. Unit 1	2747	135	0.95	0.033	0.176	0.249	0.004	0.571	0.14	0.00
10.Shell Christensen 1-33A5	3453	146	0.51	0.029	0.000	0.302	0.024	0.674	0.11	0.00
11.Shell Brotherson 1-11B4	4004	155	0.44	0.025	0.000	0.302	0.075	0.623	0.11	0.00

*Present-day burial depth

I.O.C. - Integral Oil Composition indicator - oil expected in absence of migration

D.O.C. - Differential Oil Composition indicator - oil currently being produced

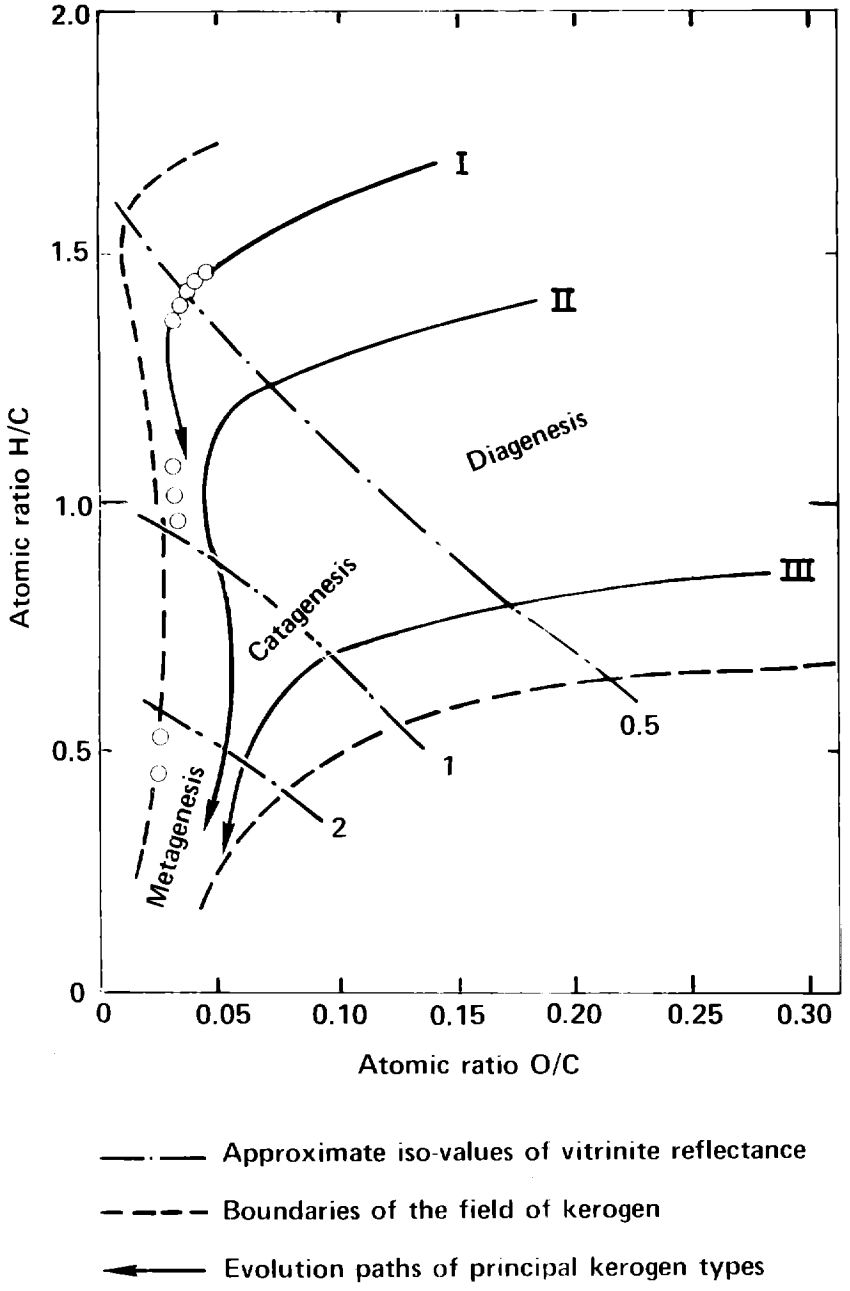

Figure 23. Van Krevelen diagram showing calculated changes in elemental composition of kerogen from the wells modeled and listed in Table 4.

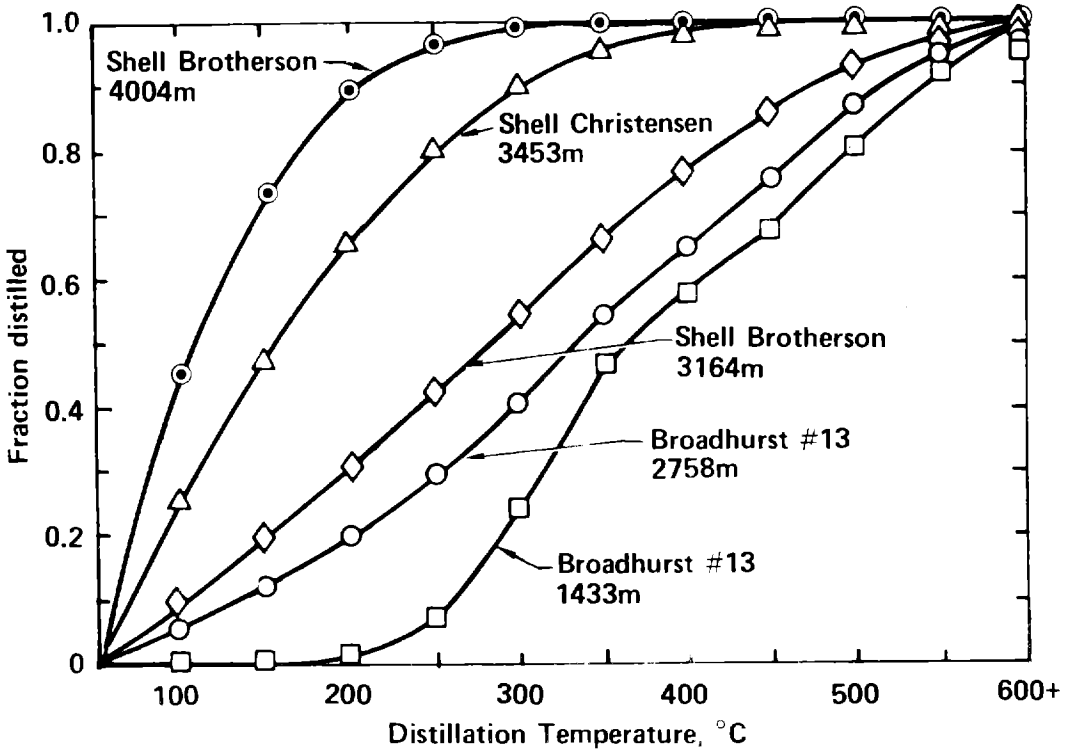

Figure 24. Boiling point distributions calculated by the model for selected wells listed in Table 4.

other oil samples cracking is probably less extensive. In this case biomarker/normal alkane ratios can be related to the extent of kerogen conversion. This provides an additional basis for comparing the geological and chemical model calculations.

At present, there is no consensus on the best method to assess the extent of kerogen conversion in organic-rich geologic materials. Advantages and disadvantages of the use of indicators such as vitrinite reflectance, thermal alteration index, and pyrolysis temperature are discussed by Anders and Gerrild (1984). There is also no standard method in practice of analyzing hydrocarbon composition; thus different investigations have different means of representing compositional data.

Three published studies (Reed and Henderson, 1971; Tissot et al., 1978; and Anders and Gerrild, 1984) give analyses of hydrocarbons at various depths from different lithologic facies in the Uinta Basin. Gas chromatograms of the hydrocarbon fractions are given by Reed and Henderson and Tissot et al. In order to compare these data with our calculations of predicted maturity (in the form of percent of oil generated), we derived cumulative and instantaneous maturity indicators from laboratory pyrolysis gas chromatographs. For indicators of maturity, we used the pristane/(C_{17} + C_{18}), phytane/(C_{17} + C_{18}), and C_{17}/(C_{16}+ C_{18}) ratios. Figures 20 and 21 are calibration curves prepared using the data of Coburn and Campbell (1977) and Burnham et al. (1982).

The data of Table 4 can be used to make another type of calibration curve. In each model, the percent of oil ungenerated, percent of liquid oil created, and the atomic H/C ratio are calculated. From this, we can determine the transformation ratio (or production index) [S_1/(S_1 + S_2)]. In the Rock-Eval pyrolysis method (commonly used in the oil industry) S_1 corresponds to the free hydrocarbons that are released between 90°C and 300°C in flowing helium. Hydrocarbons which are generated during kerogen pyrolysis between 300°C and 600°C correspond to S_2. In Table 4, the liquid oil produced is equivalent to S_1 and the oil ungenerated is equivalent to S_2. Transformation ratios for various depths in the wells in the Altamont-Bluebell field have been determined by Anders and Gerrild (1984). Figure 25, which compares the amount of kerogen converted with transformation ratio and H/C

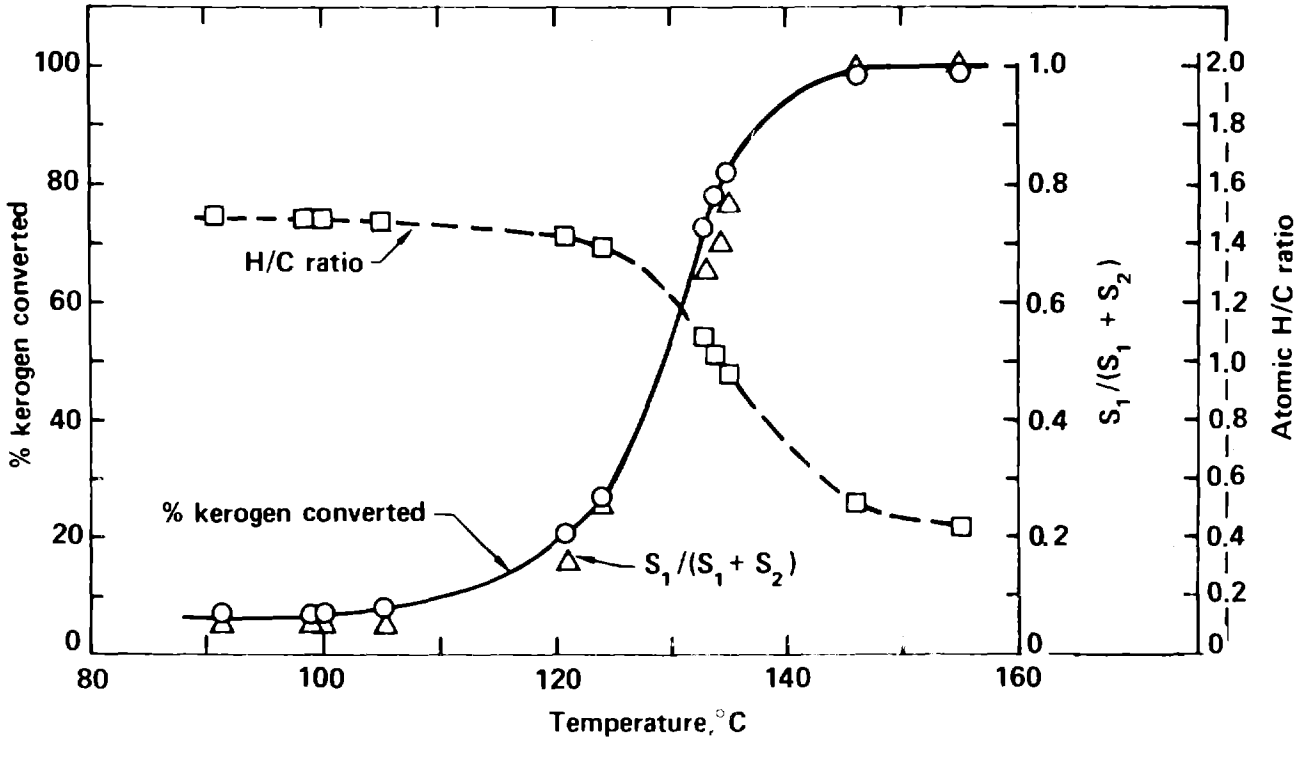

Figure 25. Calibration of transformation ratio $[S_1/(S_1 + S_2)]$ and H/C ratio with the percent of kerogen converted and maximum temperature, T_{max}, attained by the kerogen. Data points are from the model runs of Table 4.

Table 5. Comparison of hydrocarbon maturity of wells studied by Tissot et al. (1978) with model calculations. Maturity levels are estimated from the compositional ratios using Figs. 20-21.

Wells from Tissot et al. (1978).		Composition Ratios			Estimated maturity level (% oil produced)
Well Name	Depth*(m)	$\frac{\text{pristane}}{C_{17}+C_{18}}$	$\frac{\text{phytane}}{C_{17}+C_{18}}$	$\frac{C_{17}}{C_{16}+C_{18}}$	
A. Shell Brotherson 1-14B4(2S,4W)	2298	0.84	0.69	1.2	0-25%
Shell Brotherson 1-23B4(2S,4W)	2210	1.26	0.95	1.3	0-20%
Shell Brotherson 1-23B4	2557	0.58	0.58	0.5	15-35%
Shell Brotherson 1-23B4	2782	0.18	0.36	0.6	30-60%
B. Shell Murdock (2S,5W)	2982	0.23	0.20	0.6	> 40%
Shell Murdock	3552	0.09	0.05	0.5	> 60%
C. Standard of Calif. Redwash 132	2649	0.32	0.14	0.6	30-60%
Redwash 164	1698	1.46	1.90	0.6	0-20%

Models from this study for comparison					
Model Well	Depth*(m)	Z_{OB}(m)	T_{max}	Calculated H/C	Calculated maturity level (% oil produced)
A. Shell Brotherson 1-11B4 (2S,4W)	2298	1796	112°	1.40	11%
Shell Brotherson 1-11B4	2210	1796	110°	1.40	9%
Shell Brotherson 1-11B4	2557	1796	119°	1.36	20%
Shell Brotherson 1-11B4	2782	1796	125°	1.28	36%
Shell Brotherson 1-11B4	2782	2142	133°	0.99	73%
Shell Brotherson 1-11B4	2782	1547	118°	1.36	19%
B. Shell Brotherson 1-11B4	2982	1796	129°	1.14	56%
Shell Christensen (1S,5W)	2982	1987	134°	0.93	78%
Shell Brotherson 1-11B4	3552	1796	144°	0.52	99%
Shell Christensen	3552	1987	149°	0.46	100%
C. Chevron Redwash 25(7S,24E)	2649	1410	111°	1.40	10%
Broadhurst #13(7S,23E)	2649	1803	121°	1.35	24%
Chevron Redwash 250	1698	1410	88°	1.45	6%
Broadhurst #13	1698	1803	98°	1.44	7%

*present-day depth in well

ratio for a range of T_{max}, was prepared from Table 4 and is the basis for comparison of our geologic-geochemical models with published data. In each case, we assumed that the value of Z_{OB} (which determines T_{max}) is the determining variable for hydrocarbon maturation and that small changes in heating rate (due to different burial histories and different values of T_{max}) are negligible.

The data of Tissot et al. (1978) are compared with the results of our model in Table 5. Maturity levels for the published oil compositions are determined from the indicators of Figs. 20 and 21. The comparison ratios (such as $C_{17}/(C_{16} + C_{18})$), were estimated using published figures from the article. Data from the published paper are listed in the left side of the table, data calculated by our model or interpolated from Fig. 21 are listed on the right side.

The Shell Brotherson 1-11B4 well, which we modeled, is in the same section as the Shell Brotherson 1-14B4 and 1-23B4 wells used by Tissot et al. Using 1796 m for Z_{OB}, our results agree well with Tissot et al. for all four depths sampled. A range of values of Z_{OB} was used to compare the 2782 m depth sample of Shell Brotherson 1-23B4 with our model. Our estimate of maturity from Tissot et al. is 30 to 60% for this well. The low value of Z_{OB}, 1547 m, results in a 19% maturity, while the high value of Z_{OB}, 2142 m, results in a 73% calculated maturity. Both of these calculated values are out of the range by roughly equal amounts, suggesting that the value of 1796 m for Z_{OB} is a good determination for this section.

In Section B of Table 5, the Shell Murdock well data of Tissot et al., are compared to our calculations for the Shell Brotherson 1-11B4 (next section east) and Shell Christensen (next section north) wells at the different depths. In each case, the calculated values (56%, 78% and 99%, 100%) are consistent with the (>40% and >60%) values estimated from the oil composition. In this case, it is difficult to make any conclusions, except that the Z_{OB} of 1987 m from the Christensen well may be slightly high.

Wells from the Redwash area are compared in Section C of Table 5. Exact locations of the wells used by Tissot et al. are not given in their paper, so we compared their data with a range of values for Z_{OB} in the Redwash area.

For the shallower wells, the 6 to 7% calculated maturity is within the range of 0 to 20% estimated from the oil composition. Values of maturity from our calculations at the deeper levels are smaller than those which come from actual samples from the area. The highest value of Z_{OB} used, 1803 m, results in a maturity level of 24% at 2649 m, which is less than the 30 to 60% maturity indicated by the Tissot et al. data. This discrepancy would be explained if the oil sampled from the field had migrated from a more mature source area.

Recovered oil samples analyzed by Reed and Henderson (1971) are compared with results from our modeling in Table 6. The procedure is the same as for Table 5, except in this case the wells used for the model are farther away from the wells used by Reed and Henderson, so there is more extrapolation involved. In the Roosevelt area (Section A), agreement is not very good for the shallower depth. A value of Z_{OB} (or a higher value for geothermal gradient) higher than 1980 m would be needed to get the model in line with the field data. However, for the deeper sample, 3019-3043 m, agreement is good for a Z_{OB} of 1598 m. Migration may play a role at the shallower depths in this area.

In sections B, C, and D of Table 6 calculated maturity levels are consistently lower than maturity levels estimated from the actual samples. At Pariette Bench, the model predictions with the (probably high) value of 2673 m for Z_{OB} are still too low (9 to 12%) compared with 20 to 40%. This suggests that the oil in place is migrated oil, as has also been suggested by Pitman et al. (1982) and Anders and Gerrild (1984). Similarly, the highest values of Z_{OB} do not produce high enough maturity levels in the Duchesne and Redwash areas, and thus the oil there also is probably migrated oil.

We applied a method of petroleum formation analysis, described by Waples (1980), to the burial history curves for the Shell Brotherson (Fig. 4) and Pariette Bench (Fig. 5) wells. The time-temperature index (TTI) for the Shell Brotherson well we calculated is 57.8 for the 2557 m level and 101.1 for the 2782 m level. These indexes correspond roughly to maturity levels of 45% and 55%, respectively. These estimates are slightly high when they are compared to the data of Tissot et al. in Table 5. We calculate a TTI of 211.3 (100%

Table 6.

Comparison of estimated hydrocarbon maturity in wells of Reed and Henderson (1971) with model calculations. Maturity levels are estimated from the compositional ratios using Figs. 20 and 21.

Data of Reed and Henderson (1971)

Well Name	Present-day Depth(m)	Composition Ratios: pristane / C_{17} + C_{18}	Composition Ratios: phytane / C_{17} + C_{18}	Composition Ratios: C_{17} / C_{16} + C_{18}	Estimated maturity level (% oil produced)
A. Roosevelt Field Area (1S,1E)					
Roosevelt	2227-2230	0.64	0.43	0.61	15-25%
Roosevelt	3019-3034	0.30	0.27	0.58	30-40%
B. Redwash Area (7S,22E to 8S, 23E)					
W. V. Stagecoach	1547-1550	0.35	0.27	0.59	20-35%
W. V. Gypsum Hills	1608-1684	0.25	0.24	0.57	25-50%
C. Pariette Bench Area (9S, 18E)					
Pariette Bench	1478-1500	0.24	0.26	0.59	20-40%
River Junction	1322-1325	0.34	0.26	0.58	20-40%
D. Duchesne Area (3S,5W to 4S, 4W)					
Duchesne Co.	1562-1593	0.47	0.29	0.72	15-25%
Flat Mesa	2688-2774	0.08	0.04	0.53	> 80%
Indian Ridge	2245-2476	0.03	0.01	0.52	> 80%

Models from this study for comparison

Model Well	Present-day Depth(m)	Z_{OB}(m)	T_{max}	Calculated H/C	Calculated maturity level (% oil produced)
A. Roosevelt area					
Gulf Verl Johnson (1S,2W)	2225	1598	106°	1.42	8%
Gulf Ute Tribal (1N,2W)	2225	1974	115°	1.38	14%
Gulf Verl Johnson (1S,2W)	3018	1598	125°	1.28	37%
Gulf Ute Tribal (1N,2W)	3018	1974	135°	.87	82%
B. Redwash Area					
Chevron Redwash 250(7S,24E)	1524	1410	83°	1.46	0%
Broadhurst #13 (7S,22E)	1524	1803	93°	1.44	6%
Chevron Redwash 250	1676	1410	87°	1.46	0%
Broadhurst #13	1676	1803	97°	1.44	7%
Gulf Duchesne Co. (3S,4W)	1676	2252	108°	1.41	8%
C. Pariette Bench Area (9S,18E)					
Pariette Bench	1494	2673	114°	1.39	12%
Pariette Bench	1323	2673	110°	1.40	9%
D. Duchesne Area (3S,5W to 4S,4W)					
Texaco Ute Tribal (3S,6W)	1585	1878	97°	1.44	7%
Gulf Duchesne (3S,4W)	1585	2252	106°	1.42	8%
Texaco Ute Tribal	2688	1878	124°	1.30	33%
Gulf Duchesne	2688	2252	134°	0.93	78%
Texaco Ute Tribal	2377	1878	116°	1.38	15%
Gulf Duchesne	2377	2252	126°	1.26	42%

maturity) for the base of the Eocene (2250 m) in the Pariette Bench well using the Waples method - this is much higher than levels indicated in Table 6. These differences could be due to values of Z_{OB} being too high, or they may indicate that the Waples method over estimates the maturity level for this type of kerogen.

Higher values for the geothermal gradient would produce higher calculated maturity levels. In the Redwash area (Table 6, Section B) at the 1676 m level, with an assumed value for Z_{OB} of 1676 m, a geothermal gradient of 34°C/km (an increase of 9° C/km over the value used in the model) would produce a T_{max} of 124°C. The corresponding maturity level calculated with our model is about 30% (from Fig. 25) and would agree well with measured values of 20 to 40%. However, the lower values of geothermal gradient work best for the Shell Brotherson wells in the deepest part of the basin where migration is less likely. There is no geologic evidence (such as magma intrusion at depth) for large changes in geothermal gradient over such a small area, and it is unlikely that the magnitude of change required could be accounted for by hydrologic circulation. Furthermore, the nature of fracturing in the basin (Narr and Currie, 1982, Anders and Gerrild, 1984) is conducive to migration of hydrocarbons. Thus, we conclude that migration, rather than large changes in Z_{OB} or geothermal gradient, is the most likely explanation for the difference between modeled predictions and measurements of maturity levels indicated in Tables 5 and 6.

One additional comparison of predicted and sampled estimates of maturity is listed in Table 7. Anders and Gerrild (1984) sampled five wells from the Uinta Basin and compared various maturity indicators with total organic carbon (TOC) determinations and parameters such as stratigraphic facies. In Table 7 we compare our determinations of the transformation ratio (from values of Z_{OB} with a 25°C/km geothermal gradient and using Fig. 25) with those determined from sampled material by Anders and Gerrild.

Agreement of our predictions with real data for the Dustin #1 well (compared using a Z_{OB} of 1868 m determined for the Ute Tribal B-7 well) is good for depths shallower than 2926 m. Our model predicts higher values of transformation ratio for greater depths. It is impossible for maturity to

Table 7.

Comparison of hydrocarbon maturity of wells studied by Anders and Gerrild (1984) with model calculations.

Wells from Anders and Gerrild (1984)			Results from this study: Transformation ratio estimated from Fig. 25.			
Well Name	Depth (m)	Measured $S_1/(S_1+S_2)$	Model Well	Depth (m)	T_{max}	$\frac{S_1}{(S_1+S_2)}$
Dustin #1(2S,3W)	2591	.13	Ute Tribal 6-7(2S,3W)	2591	121°	.18
"	2701	.19	Z_{OB}=1868 m	2701	124°	.26
"	2926	.70	"	2926	130°	.57
"	3353	.61	"	3353	141°	.92
"	4054	.61	"	4054	158°	1.00
Daniel Uresk (4S,1W)	1524	.07	Gulf Duchesne(3S,4W)	1524	104°	.11
"	2091	.17	Z_{OB}=2252 m	2091	119°	.14
"	2377	.43	"	2377	126°	.35
"	2926	.12	"	2926	139°	.88
"	3374	.07	"	3374	151°	1.00
WOSCO EX-1(9S,20E)	610	.09	Pariette Bench(9S,18E)	610	92°	.05
"	853	.01	Z_{OB}=2673 m	853	98°	.05
Cedar Rim #3 (3S,6W)	1402	.05	Ute Tribal E-1(3S,6W)	1402	92°	.05
"	1951	.07	Z_{OB}=1878 m	1951	106°	.06
"	2256	.08	"	2256	113°	.07
Ute Tribal 1-16 (4S,7W)	2134	.16	Ute Tribal E-1(3S,6W)	2134	110°	.06
"	2286	.17	Z_{OB}=1878 m	2286	114°	.09
"	2377	.18	"	2377	116°	.10
			Gulf Duchesne(3S,4W)	2134	120°	.14
			Z_{OB}=2252 m	2286	123°	.22
			"	2377	126°	.36

decrease with increased depth. The discrepancy must be caused by migration. This suggests that most of the oil at 2926 m and 3374 m must have either migrated or cracked. Results are similar for the Daniel Uresk well (compared using a Z_{OB} of 2225 m). Hydrocarbon samples from the Wosco Ex-1 and CEDAR RIM #3 wells are very immature, in complete agreement with our modeling. Our model of the Ute Tribal 1-16 predicts maturity levels that are low for Z_{OB} = 1870 m and high, but close, for Z_{OB} = 2252 m. This suggests (assuming the geothermal gradient used is correct) that a value of 2134 m of overburden removed is more reasonable for the area of the Ute Tribal 1-16 well.

V. Summary and Conclusions

Using geophysical log data and present-day values of the geothermal gradient, we have developed a model of the thermal history of stratigraphic marker horizons for selected wells in the Uinta Basin. We incorporated thermal-history data into a pyrolysis model to predict the amounts of hydrocarbons produced and indicators of their maturity level as the kerogen was thermally evolved. For a geothermal gradient that is spatially and temporally constant, the controlling variable in the thermal history model is the amount of overburden removed by erosion.

Predicted maturity levels of the evolved hydrocarbons in the basin agree well with measured maturity levels. We feel that this agreement gives us confidence in the general applicability of a laboratory-based pyrolysis model to geological processes. While the present model is valid only for Type I kerogen, it seems certain that a similar model could be developed for Type II and Type III kerogens. We emphasize the following conclusions:

- The value of activation energy (52.4 kcal/mole) used in the pyrolysis model results in good prediction of amounts and compositions of evolved hydrocarbons in the deepest part of the basin.

- Discrepancies between predicted and measured maturity levels in the Redwash and Pariette Bench areas are probably related to migration.

- Estimated values for removed overburden of approximately 1800 m in the Shell Brotherson 1-11B4 well area result in very good agreement between predicted and measured maturity levels, and this value of Z_{OB} is constrained by about ± 150 m by the model (assuming a constant geothermal gradient).

- If reasonable values for overburden removed are limited to being less than 2750 m and greater than 900 m, the geothermal gradient would have had to be about 10°C/km (40%) greater in the Duchesne River, Redwash, and Pariette Bench areas to account for the difference between predicted and measured maturity levels with no migration of hydrocarbons.

In the process of this investigation we feel that we have gained much insight into the natural kerogen conversion process as well as the nuances of the pyrolysis model. By incorporating the ability to vary pressure in the pyrolysis model (in future work) and adding calculations of pore volumes and pressures, the true potential for geological application of the model can be realized. Utilization of a refined pyrolysis model with more detailed geologic data and models will enable us to study the phenomena of migration and overpressuring in detail. Refinement of these techniques and study of other geologic basins could eventually lead to the use of the pyrolysis model in quantitative evaluations of the thermal history of sedimentary basins and the associated hydrocarbon resource potential.

Acknowledgment

Development of the pyrolysis model was made possible through support by the Oil Shale and Basic Energy Science programs at Lawrence Livermore National Laboratory. The initial impetus for this project came from Dr. A. E. Lewis. Dr. J. Younker greatly expanded the ideas of how to couple the geological and chemical models. Discussions with and suggestions from Dr. David Andersen and Dr. David Chapman were very helpful. Reviews and suggestions by Fred Meissner, Bird Oil Corp., Dr. David Andersen, San Jose State U., and Dr. Douglas Waples helped improve the manuscript. Drafting work by P. Proctor is much appreciated. Word processing was expertly done by Dianne Mc Govern.

REFERENCES

Anders, D. E. and Gerrild, P. M., 1984, "Hydrocarbon Generation in Lacustrine Rocks of Tertiary Age, Uinta Basin, Utah - Organic Carbon, Pyrolysis Yield, and Light Hydrocarbons," Hydrocarbon Source Rocks of the Greater Rocky Mountain Region, J. Woodward, F. F. Meissner, and J. L. Clayton, eds., Rocky Mountain Association of Geologists, Denver, pp. 513-529.

Andersen, D. W., and Picard, M. D., 1974, "Evolution of Synorogenic Clastic Deposits in the Intermontane Uinta Basin of Utah," SEPM Sp. Publ. 22: Tectonics and Sedimentation, W. R. Dickinson, ed., pp. 167-189.

Anthony, D. B. and Howard, J. B., 1976, "Coal Devolatilization and Hydrogasification," AIChE J., Vol. 22, p. 625

Bond, G. C., and Kominz, M. A., 1984, "Construction of Tectonic Subsidence Curves for the Early Proterozoic Miogeocline, Southern Canadian Rocky Mountains: Implications for Subsidence Mechanisms, Age of Breakup, and Crustal Thinning," G.S.A. Bull, Vol. 95, No. 2, pp. 226-236.

Bradley, W. H., 1925, "A Contribution to the Origin of the Green River Formation and its Oil Shale," AAPG Bull, Vol. 9, pp. 247-262.

Bradley, W. H., 1929, The Varves and Climate of the Green River Epoch, U.S.G.S. Prof. Paper 158-E, pp. 87-110.

Bradley, W. H., 1931, Origin and Microfossils of the Oil Shales of the Green River Formation of Colorado and Utah, U. S. Geological Survey Prof. Paper 168, 58 p.

Bradley, W. H., 1970, "Green River Oil Shale - Concept of Origin Extended," G.S.A. Bull., Vol. 81, pp. 985-1000.

Burnham, A. K., 1981, "Chemistry of Shale Oil Cracking," Oil Shale, Tar Sands and Related Materials, ACS Symposium Series 163, H. C. Stauffer, Ed., Washington, DC, p. 39.

Burnham, A. K. and Braun, R. L., 1985, "General Kinetic Model of Oil Shale Pyrolysis," In Situ, Vol. 9, No. 1, pp. 1-23.

Burnham, A. K. and Singleton, M. F., 1983, "High-pressure Pyrolysis of Green River Oil Shale," Chemistry and Geochemistry of Oil Shale, ACS Symposium Series 230, F. P. Miknis, ed., American Chemical Society Washington, D.C. p. 335.

Burnham, A. K., Clarkson, J. E. Singleton, M. F., Wong, C. M., and Crawford, R. W., 1982, "Biological Markers from Green River Kerogen Decomposition," Geochimica et Cosmochimica Acta, v. 46, pp. 1243-1251.

Campbell, J. H., Gallegos, G., and Gregg, M., 1980, "Gas Evolution During Oil Shale Pyrolysis. 2. Kinetic and Stoichiometric Analysis," Fuel, Vol. 59, pp. 727-732.

Campbell, J. H., Koskinas, G. J., and Stout, N. D., 1978a, "Kinetics of Oil Generation from Colorado Oil Shale," Fuel, Vol. 57, No. 6, pp. 372-376.

Campbell, J. H., Koskinas, G. J., Stout, N. D., and Coburn, T. T., 1978b, "Oil Shale Retorting: Effects of Particle Size and Heating Rate on Oil Evolution and Intra-particle Oil Degradation," In Situ, Vol. 2, No. 1, pp. 1-47.

Carmichael, R. S., ed., 1982, "Handbook of Physical Properties of Rocks, Volume II," CRC Press, Inc., Boca Raton, Fla, 345 pp.

Chapman, D. S., Keho, T. H., Bauer, M. S., and Picard, M. D., 1984, "Heat Flow in the Uinta Basin Determined from Bottom Hole Temperature (BHT) Data," Geophysics, Vol. 49, No. 4, pp. 455-466.

Chatfield, J. 1972, "Case History of Redwash Field, Uinta County, Utah," in Stratigraphic Oil and Gas Fields, R. E. King, ed., AAPG Memoir No. 16, pp. 342-353.

Coburn, T. T. and Campbell, J. H., 1977, "Oil Shale Retorting: Part II, Variation in Product Oil Chemistry During Retorting of an Oil Shale Block," Lawrence Livermore National Laboratory Report UCRL-52256, pt. 2.

Connan, J., 1974, "Time-Temperature Relation in Oil Genesis," AAPG Bull., Vol. 58, no. 12, pp. 2516-2521.

Fouch, T. D., 1975, "Lithofacies and Related Hydrocarbon Accumulations in Tertiary Strata of the Western and Central Uinta Basin," Symposium on Deep Drilling Frontiers in the Central Rocky Mountains, D. W. Bolyard, ed., Rocky Mountain Assn. Geol. Spec. Publ., pp. 163-173.

Fouch, T. D., 1981, Distribution of rock types, lithologic groups, and interpreted depositional environments for some lower Tertiary and upper Cretaceous rocks from outcrops at Willon Creek-Indian Canyon through the subsurface of Duchesne and Altamont oil fields, southwest to north central parts of the Uinta Basin, Utah, USGS Oil and Gas Investigation Map, Chart OC-81.

Fouch, T. D., and Cashion, W. B., 1979, Preliminary chart showing distribution of rock types, lithologic groups and depositional environments for some lower Tertiary, upper and lower Cretaceous and upper and middle Jurassic rocks in the subsurface between Altamont oil field and San Arroyo gas field, north central to southeastern Uinta Basin, Utah, USGS Open-File Report 79-365, 2 sheets.

Hansen, W. R., 1984, "Post-Laramide Tectonic History of the Eastern Uinta Mountains, Utah, Colorado, and Wyoming," The Mountain Geologist, Vol. 21, No. 1, pp. 5-29.

Hunt, J. M., 1979, Petroleum Geochemistry and Geology, W. H. Freeman and Co., San Francisco, 617 pp.

Ishiwatari, R., Ishiwatari, M., Kaplan, I. R., and Rohrback. B. G., 1976, "Thermal Alteration of Young Kerogen in Relation to Petroleum Genesis," Nature, Vol. 264, pp. 347-49.

Lucas, P. T., and Drexler, J. M., 1975, "Altamont-Bluebell: A Major Fractured and Overpressured Stratigraphic Trap, Uinta Basin, Utah," Deep Drilling Frontiers of the Central Rocky Mountains, D. W. Bolyard, ed., Rocky Mt. Assn. of Geologists Symposium, pp. 265-273.

Magara, K., 1978, Compaction and Fluid Migration - Practical Petroleum Geology, Elsevier, New York, pp. 11-25.

Mauger, R. L., 1977, "K-Ar Ages of Biotites from Tuffs in Eocene Rocks of the Green River, Washakie, and Uinta Basins, Utah, Wyoming, and Colorado," Contributions to Geology, University of Wyoming, Vol. 15, No. 1, pp. 17-41.

Meissner, F., 1982, Basin Geochemistry - Case Histories, Notes from AAPG Geochemistry for Geologists School, Houston, TX, October 4-6, 1982.

Narr, W. and Currie, J. B., 1982, "Origin of Fracture Porosity - Example From Altamont Field, Utah," AAPG Bull., Vol. 66, No 9, pp. 1231-1247.

Palmer, A. R., 1983, "The Decade of North American Geology 1983 Geologic Time Scale," Geology, Vol. 11, pp. 503-504.

Philippi, G. T., 1965, "On the Depth, Time, and Mechanisms of Petroleum Generation," Geochimica et Gosmochimica Acta, Vol. 25, pp. 1021-1049.

Pitman, J. K., Fouch, T. D., and Goldhaber, M. B., 1982, "Depositional Setting and Diagenetic Evolution of Some Tertiary Unconventional Reservoir Rocks, Uinta Basin, Utah," AAPG Bull, Vol. 66, No. 10, pp. 1581-1596.

Reed, W. E. and Henderson, W., 1971, "Proposed Stratigraphic Controls on the Composition of Crude Oils Reservoired in the Green River Formation, Uinta Basin, Utah," Advances in Geochemistry, Pergamon Press, Oxford, pp. 499-515.

Robinson, W. E., 1969, "Kerogen of the Green River Formation," Organic Geochemistry, G. Eglington and M. T. J. Murphy eds., Springer-Verlag, New York, pp. 619-637.

Ryder, R. T., Fouch, T.D., Elison, J. H., 1976, "Early Tertiary Sedimentation in the Western Uinta Basin, Utah," GSA Bull., Vol. 87, pp. 496-512.

Saxby, J. D. and Riley, K. W., 1984, "Petroleum Generation by Laboratory-scale Pyrolysis Over Six Years Simulating Conditions in a Subsiding Basin," Nature, Vol. 308, March 8, pp. 177-179.

Sclater, J. G. and Christie, P. A. F., 1980, "Continental Stretching: An Explanation of the Post Mid-Cretaceous Subsidence of the Central North Sea Basin," Journ. Geophys. Res., Vol. 85, No. 87, pp. 3711-3739.

Shih, S. M. and Sohn, H. Y., 1980, "Nonisothermal Determination of the Intrinsic Kinetics of Oil Generation from Oil Shale," Ind. Eng. Chem. Proc. Des. Dev., Vol. 19, p. 420.

Smith, J. W., 1974, "Geochemistry of Oil-Shale Genesis in Colorado's Piceance Creek Basin," Rocky Mtn. Assn. of Geologists Guidebook, pp. 71-79.

Steckler, M. S. and Watts, A. B., 1978, "Subsidence of the Atlantic-type Continental Margin off New York," Earth and Planet. Sci. Ltrs., Vol. 41, pp. 1-13.

Stokes, W. L., 1973, Geologic Map of Utah, College of Mines and Mineral Industries, University of Utah, 2 sheets.

Stout, N. D., Koskinas, G. J., Raley, Santor, S. D., Opila, R. J., and Rothman, A. J., 1976, "Pyrolysis of Oil Shale: The Effects of Thermal History on Oil Yield," Proceedings 9th Oil Shale Symposium, Colorado School of Mines, Golden, Colorado.

Tissot, B., Deroo, G., and Hood, A., 1978, "Geochemical Study of the Uinta Basin: Formation of Petroleum from the Green River Formation," Geochim. Cosmochim. Acta, Vol. 42, pp. 1469-1485.

Tissot B. P. and Welte, D. H., 1978, Petroleum Formation and Occurrence, Springer-Verlag, New York, 538 pp.

Tissot, B. and Espitalie, J., 1965, "L'evolution Thermique de la Matiere Organique des Sediments; Applications d'une Simulation Mathimatique Potential Petrolier des Bassins Sedimentaires et Reconstitution de L'histore Thermique des Sediments," Revere de l'Institut Francais de Petrole, Vol. 30, pp. 743-777.

Van Heek, K. H. and Juntgen, H. 1968,"Determination of Reaction-Kinetic Parameters from Nonisothermal Measurements," Ber. Bensenges. Physik. Chem., V. 72, p. 1223; available as English Translation in Lawrence Livermore National Laboratory rept. UCRL-TRANS-10974 (1975).

Waples, D. W., 1980, "Time and Temperature in Petroleum Formation-Application of Lopatin's Method to Petroleum Exploration," AAPG Bull, V. 64, pp. 916-926.

Yen, T. G. and Chilingarian, G. V., eds., 1976, Oil Shale, Elsevier, Amsterdam.